Polytechnic
UNIVERSITY

Final Report

to

U.S. Army Research Office

4300 South Miami Boulevard

P.O. Box 12211

Research Triangle Park, NC 27709-2111

for

Grant # DAAD19-99-1-0278

Radio Wave Propagation in Tunnels

Prepared by

Jeho Lee

and

Henry L. Bertoni

Polytechnic University

6 MetroTech Center

Brooklyn, NY 11201

March 15, 2000

REPORT DOCUMENTATION PAGE

Form Approved
OMB NO. 0704-0188

1. AGENCY USE ONLY *(Leave blank)*	2. REPORT DATE	3. REPORT TYPE AND DATES COVERED
	March 15, 2000	Final

4. TITLE AND SUBTITLE

Radio Wave Propagation in Tunnels

5. FUNDING NUMBERS

DAAD19-99-1-0278

6. AUTHOR(S)

Jeho Lee and Henry L. Bertoni

7. PERFORMING ORGANIZATION NAMES(S) AND ADDRESS(ES)

Polytechnic University
Brooklyn, NY 11201

8. PERFORMING ORGANIZATION REPORT NUMBER

9. SPONSORING / MONITORING AGENCY NAME(S) AND ADDRESS(ES)

U.S. Army Research Office
P.O. Box 12211
Research Triangle Park, NC 27709-2211

10. SPONSORING / MONITORING AGENCY REPORT NUMBER

ARO 39776.1-EL-II

11. SUPPLEMENTARY NOTES

The views, opinions and/or findings contained in this report are those of the author(s) and should not be construed as an official Department of the Army position, policy or decision, unless so designated by other documentation.

12a. DISTRIBUTION / AVAILABILITY STATEMENT

Approved for public release; distribution unlimited.

12 b. DISTRIBUTION CODE

13. ABSTRACT *(Maximum 200 words)*

This report examines the radio propagation model for narrow and long tunnels. Modal analysis is used to model the path gain in 2-D and 3-D rectangular tunnels and the coupling loss of L, T and cross tunnels. Modal attenuation is determined by the wavelength λ and given tunnel dimension through the factor λ^2/w^3, where w is the width of tunnel, by the mode number and dielectric constant of the walls. In oversized

14. SUBJECT TERMS			15. NUMBER IF PAGES
			16. PRICE CODE
17. SECURITY CLASSIFICATION OR REPORT	18. SECURITY CLASSIFICATION OF THIS PAGE	19. SECURITY CLASSIFICATION OF ABSTRACT	20. LIMITATION OF ABSTRACT
UNCLASSIFIED	UNCLASSIFIED	UNCLASSIFIED	UL

tunnels, many modes may propagate, however higher modes have high attenuation constant so that a few lower modes are dominant at long distances from the transmitter. The antenna polarization, giving the least path loss in 3-D tunnels, is found by comparing attenuation constants of both vertical and horizontal polarization. For the propagation into branches off the main tunnel, mode coupling at the discontinuities is obtained by hybrid ray-mode conversion. By accounting for the mode diffraction at each corner, we compute the coupling loss into cross junctions, the T-junction and L-bends. Because the cross tunnel has four edges and they generate more corner diffracted modal fields than other structures, and have the strongest coupling. The coupling loss is found to increase slightly with tunnel width.

Abstract

This report examines the radio propagation model for narrow and long tunnels. Modal analysis is used to model the path gain in 2-D and 3-D rectangular tunnels and the coupling loss of L, T and cross tunnels. Modal attenuation is determined by the wavelength λ and given tunnel dimension through the factor λ^2/w^3, where w is the width of tunnel, by the mode number and dielectric constant of the walls. In oversized tunnels, many modes may propagate, however higher modes have high attenuation constant so that a few lower modes are dominant at long distances from the transmitter. The antenna polarization, giving the least path loss in 3-D tunnels, is found by comparing attenuation constants of both vertical and horizontal polarization. For the propagation into branches off the main tunnel, mode coupling at the discontinuities is obtained by hybrid ray-mode conversion. By accounting for the mode diffraction at each corner, we compute the coupling loss into cross junctions, the T-junction and L-bends. Because the cross tunnel has four edges and they generate more corner diffracted modal fields than other structures, and have the strongest coupling. The coupling loss is found to increase slightly with tunnel width.

Contents

1. Introduction

Radio communication in mine, rail and road tunnels has been of interest since 1920s. Early studies considered the use of leaky cables, which are widely used to provide relatively uniform coverage over a tunnel [1]. However the use of leaky cables requires prior access to the tunnel in order to install the cable and related infrastructure. Free propagation between radio transceivers has also been studied. In this case the tunnel acts as lossy waveguide. Both modal [2] and ray [3,4,5] approaches have been used to model propagation in tunnels, as discussed below.

For small tunnels and at lower frequencies, the tunnel dimensions are only a few times the wavelength of the radio signal. In this case the modal approach is simpler and more accurate. For long distance along a straight tunnel, the modal approach is appropriate even when the tunnel dimensions are much larger than the wavelength. The purpose of this study is to evaluate the coupling of such modes at junctions and bends in tunnels.

For the modal analysis approach to propagation, the tunnel is treated as a hollow wavegude with lossy dielectric walls. Mahmound and Wait [6] studied the radiation of dipoles in rectangular tunnel assuming the side walls to be perfectly conducting. Emslie et. al. [2] found approximate mode solutions for the propagation constant and the field distribution in straight tunnels with dielectric walls. Numerical evaluation of the couplings at L-bends and T-junctions were carried out by Sakai and Koshiba [7] using the boundary-element method. Their approach gives the electromagnetic field distribution for two-dimensional tunnels (analogue to to parallel plate waveguide). However, this numerical approach does not yield analytic expressions for the mode coupling that explicitly contain the dependence on geometry, frequency and polarization. Mariage et al. [8] investigated field variation inside or near a tunnel entrance using the uniform theory of diffraction (UTD) to explain the coupling between free space and the tunnel. The UTD approach does result in analytic expressions. In what follows, we make use of the UTD approach to describe coupling between modes at tunnel junctions and sharp bends.

In a tunnel whose size is very large relative to the wavelength, another approach to propagation modeling is based on ray tracing. Using a 3-D ray launching approach, Cichon et. al. [3,4] studied the radio channel characteristics of various tunnels. Chen and Jeng [5] proposed studying propagation in tunnels with traffic by the shooting and bouncing ray method. Ray tracing is a very powerful method to model the wireless channel at high frequencies when the entire geometry of the tunnel is taken into account. However, for long relatively narrow tunnels many multiply reflected rays must be taken into account. Moreover, the ray tracing approach does not separate the effects of individual junctions or bends. In order to explain the propagation characteristics of long and narrow tunnel and low operating frequencies, we make use of modal analysis. We derived the modal fields and their excitation by source starting with a rigorous integral formulate for a straight tunnel. Coupling at junctions and bends is then treated using hybrid ray-mode theory to find the equivalent sources to represent the mode coupling that results from diffraction at the appropriate corners. This approach is similar to study reflection at the open end of a perfectly conducting waveguide [9], but must account for the angle dependence of the reflection coefficient.

We start by considering the simplified case of a 2-D tunnel (analogues to parallel plate waveguide) and then show how the resulting expressions are generalized to the case of actual 3-D tunnel.

2. Modal Analysis of the Radio Propagation in 2-D Straight Tunnels

2.1 Analysis of TE Propagation in 2-D Tunnels

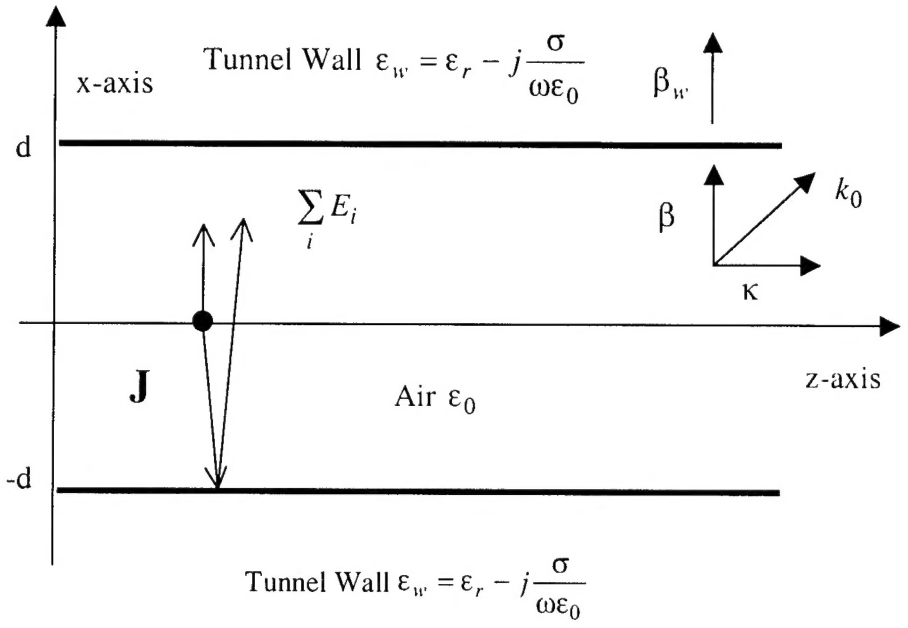

Figure 2-1. Propagation in 2-D Straight Tunnel

Consider propagation in simple 2-D tunnel shown in Figure 2-1. The side walls have the dielectric constant ε_w and finite conductivity σ. Suppose a line source of current source is located at $x = x'$ and $z = 0$ so that the current density is

$$J = a_y J_0 \delta(x - x')\delta(z) \tag{2-1}$$

The field due to the line source excitation can be found

$$\nabla \times E = -j\omega\mu H \tag{2-2}$$

$$\nabla \times H = j\omega\varepsilon E + J \tag{2-3}$$

Substituting expression (2-1) for the current gives

$$\nabla \times H = j\omega\varepsilon E + a_y J_0 \delta(x - x')\delta(z) \tag{2-4}$$

By taking the curl of both side of (2-2) and using (2-4), we obtain

$$\nabla \times (\nabla \times E) = -j\omega\mu(\nabla \times \underline{H}) = -j\omega\mu\left(j\omega\varepsilon \underline{E} + a_y J_0 \delta(x - x')\delta(z)\right) \tag{2-5}$$

The curl operations can be expanded as

$$\nabla \times (\nabla \times E) = \nabla(\nabla \cdot E) - \nabla^2 E = -\nabla^2 E \tag{2-6}$$

Since $\nabla \cdot E = 0$, from (2-5) and (2-6) we obtain the wave equation.

$$-\nabla^2 E + k^2 E = -j\omega\mu J_0 \delta(x - x')\delta(z)a_y \tag{2-7}$$

where $k = \omega\sqrt{\mu\varepsilon}$ is the wavenumber which is different in the media.

The solution of the equation (2-7) can be found using the Fourier representation of the modal field in tunnel. Since E is seen from (2-7) to have only a y-component, the Fourier representation takes the form.

$$E_y(x,z) = \frac{1}{2\pi}\int_{-\infty}^{\infty} E(x,\kappa)e^{-j\kappa z} d\kappa \tag{2-8}$$

where κ is the wavenumber along z. Conversely, $E(x,\kappa)$ is found from the Fourier transform.

$$E(x,\kappa)=\int_{-\infty}^{\infty}E_y(x,z)e^{j\kappa z}dz \tag{2-9}$$

Taking the Fourier transform of both side of the equation (2-7),

$$\int_{-\infty}^{\infty}\left[-\nabla^2 E_y+k^2E_y\right]e^{j\kappa z}dz=\int_{-\infty}^{\infty}\left[-j\omega\mu J_0\delta(x-x')\delta(z)\right]e^{j\kappa z}dz=-j\omega\mu J_0\delta(x-x') \tag{2-10}$$

Substituting equation (2-8) for $E_y(x,z)$ into (2-10), after some manipulation we obtain

$$\left(-\frac{\partial^2}{\partial x^2}+\kappa^2\right)E(x,\kappa)=-j\omega\mu J_0\delta(x-x') \tag{2-11}$$

To satisfy (2-11), $E(x,\kappa)$ must be continuous at $x=x'$, but its derivative is discontinuous above the plane $x=x'$ and below the plane in the absence of the walls. The derivative must satisfy the jump condition.

$$\frac{\partial}{\partial x}E(x,\kappa)\Big|_{x'-}^{x'+}=-j\omega\mu J_0 \tag{2-12}$$

The electric fields are given by

$$E^+(x,\kappa)=E_0(\kappa)e^{-j\beta(x-x')} \quad \text{for } x > x' \tag{2-13}$$

and

$$E^-(x,\kappa)=E_0(\kappa)e^{j\beta(x-x')} \quad \text{for } x < x' \tag{2-14}$$

where $\beta=\sqrt{k^2-\kappa^2}$ is the wavenumber along x.

$$E(\kappa)=\frac{\omega\mu}{2\beta}J_0 \tag{2-15}$$

The fields (2-13) and (2-14) may be viewed as plane waves radiated by the line source. These waves are multiply reflected by the tunnel walls. The total field E can therefore be found by summing all of the multiply reflected plane waves.
From Figure 2-1 the transform $E(x,\kappa)$ for $x > x'$ is therefore

$$E(x,\kappa)=\{e^{-j\beta(x-x')}+\left(e^{j\beta(x+x')}+e^{-j\beta(x+x')}\right)\sum_{1,3,5,\cdots}\left(\Gamma e^{-j2\beta l}\right)^m$$

$$+\left(e^{j\beta(x-x')}+e^{-j\beta(x-x')}\right)\sum_{2,4,\cdots}\left(\Gamma e^{-j2\beta l}\right)^m\}\frac{\omega\mu}{2\beta}J_0 \tag{2-16}$$

The first term in the brackets represents the wave propagating directly from the source plane $x=x'$ to the receiver plane. The second term represents waves that undergo an odd number of reflections in the tunnel walls, initially propagating upward from the source and downward towards the observation point, or downward from the source and upward to the observation point. The last term represents waves that propagate downward from the source and, upward to observation point, and upward thus experience an even number of reflection in the wall. The power series may be summed in closed form to give

$$E(x,\kappa)=\left\{\frac{e^{-j\beta(x-x')}+2\cos\beta(x+x')\Gamma e^{-j2\beta l}+\Gamma^2 e^{-j4\beta l}e^{j\beta(x-x')}}{1-\Gamma^2 e^{-j4\beta l}}\right\}\frac{\omega\mu}{2\beta}J_0 \tag{2-17}$$

2.2 Eigenvalues of the Propagation Modes in a 2-D Tunnel

Using the Fourier representation (2-8), we can express the fields radiated by a vertical polarized antenna into a straight 2-D tunnel as

$$E_y(x,z)=\frac{1}{2\pi}\int_{-\infty}^{\infty}\left\{\frac{e^{-j\beta(x-x')}+2\cos\beta(x+x')\Gamma e^{-j2\beta d}+\Gamma^2 e^{-j4\beta d}e^{j\beta(x-x')}}{1-\Gamma^2 e^{-j4\beta d}}\frac{\omega\mu}{2\beta}J_0\right\}e^{-j\kappa z}d\kappa \tag{2-18}$$

The modes are from the pole singularities of the (2-18) and are the solutions of the transverse resonance equation.

$$\Gamma^2 = e^{j4\beta d} \tag{2-19}$$

For TE mode (Vertical Polarization), the reflection coefficient is

$$\Gamma^{TE}=\frac{\frac{\omega\mu}{\beta_w}-\frac{\omega\mu}{\beta}}{\frac{\omega\mu}{\beta_w}+\frac{\omega\mu}{\beta}}=\frac{\beta-\beta_w}{\beta+\beta_w} \tag{2-20}$$

where $\beta=\sqrt{k_0^{\,2}-\kappa^2}$ is the transverse wavenumber in air region and $\beta_w=\sqrt{\varepsilon_w k_0^{\,2}-\kappa^2}$ is the transverse wavenumber in dielectric wall region.

Because the fields in the tunnel are the sum of inhomogeneous plane waves the experienced small attenuation along z, β and β_w will be nearly real and Γ^{TE} will be close to –1. In this case the solutions for β of the transverse resonance equation (2-20) will be close to $\frac{n\pi}{2d}$ for n=1,2,3, ….. .

In the view of the foregoing discussion, let

$$\beta=\frac{n\pi}{2d}-\delta \tag{2-21}$$

Substituting (2-21) into the left handside of (2-19), the transverse resonance equation becomes

$$\Gamma^2 = e^{-j4d\delta} \tag{2-22}$$

Since Γ is near -1 for the low attenuation modes, taking the square root of (2-22) gives

$$\Gamma^{TE} = -e^{-j2d\delta} \approx -(1 - j2d\delta) \tag{2-23}$$

Now consider the Taylor expansion of Γ^{TE} about $\delta = 0$. Since $\beta_w = \sqrt{(\varepsilon_w - 1)k_0^{\,2} + \beta^2}$, the first two terms in the expansion are

$$\Gamma^{TE} = \Gamma^{TE}(\delta = 0) + \delta \frac{2(\beta - \beta_w)}{\beta_w(\beta + \beta_w)} \tag{2-24}$$

In (2-24), $\beta = \dfrac{n\pi}{2d}$ and $\beta_w = \sqrt{(\varepsilon_w - 1)k_0^{\,2} + \left(\dfrac{n\pi}{2d}\right)^2}$. Equating (2-23) and (2-24), we may solve for δ and obtain the modal solutions.

$$\delta_n = \frac{1 + \Gamma^{TE}(\delta = 0)}{2\left[jd - \dfrac{\beta - \beta_w}{\beta_w(\beta + \beta_w)}\right]} = \frac{\dfrac{2\beta}{\beta + \beta_w}}{2\left[jd - \dfrac{\beta - \beta_w}{\beta_w(\beta + \beta_w)}\right]} = \frac{\beta\beta_w}{\beta_w - \beta + jd\beta_w(\beta + \beta_w)} \tag{2-25}$$

In the denominator of (2-25), $\beta_w d >> 1$ so we may further approximate the solution as

$$\delta_n \approx \frac{\beta}{jd(\beta + \beta_w)} = \frac{1}{jd\left(1 + \dfrac{\beta_w}{\beta}\right)} = \frac{1}{jd\left(1 + \sqrt{1 + (\varepsilon_w - 1)\left(\dfrac{2dk_0}{n\pi}\right)^2}\right)} \tag{2-26}$$

For the lower modes $2dk_0 >> n\pi$, and hence

$$\delta_n \approx \frac{n\pi/2dk_0}{jd\sqrt{\varepsilon_w - 1}} = \frac{n\lambda}{j4d^2\sqrt{\varepsilon_w - 1}} \tag{2-27}$$

Substituting (2-27) into (2-22) gives the poles of the integrand in (2-18)

$$\beta_n = \frac{n\pi}{2d} + j\frac{n\lambda}{4d^2\sqrt{\varepsilon_w - 1}} \tag{2-28}$$

The wavenumber along z for the n^{th} mode is then given by

$$\kappa_n = \sqrt{k_0{}^2 - \beta_n{}^2} \tag{2-29}$$

Since the imaginary part β_n is small, κ_n may be approximated

$$\kappa_n \approx \sqrt{k_0{}^2 - \left(\frac{n\pi}{2d}\right)^2} - j\frac{1}{\sqrt{k_0{}^2 - \left(\frac{n\pi}{2d}\right)^2}}\frac{n^2\pi\lambda}{4d^3\sqrt{\varepsilon_w - 1}} \tag{2-30}$$

From (2-30) it is seen that since $d >> \lambda$, the attenuation constant is approximately proportional $\frac{n^2\lambda^2}{d^3}$. Assuming that $d >> \lambda$, for the lower modes having $\frac{n\pi}{2d} << \frac{2\pi}{\lambda}$, κ_n can be further approximated as

$$\kappa_n \approx k_0 - j\frac{(n\pi)^2}{2d^3k_0{}^2\sqrt{\varepsilon_w - 1}} \tag{2-30A}$$

where ε_w is now taken to be the real part of the dielectric constant of the wall.

2.3 Modal Fields for TE Polarization in a 2-D Tunnel

The modal representation for the field in a 2-D tunnel is obtained by deforming the contour of integration in (2-18) so as to capture the poles representing the waveguide modes. To do so, it is convenient to change the variable of the integration (2-18) from κ to β. Since $\kappa = \sqrt{k_0^2 - \beta^2}$, differentiation of both sides, gives

$$d\kappa = \frac{-\beta}{\sqrt{k_0^2 - \beta^2}} d\beta \tag{2-31}$$

Thus the integration of (2-18) becomes

$$E_y(x,z) = -\frac{\omega\mu_0}{4\pi} J_0 \int_{-\infty}^{\infty} F(x,x',\beta) d\beta \tag{2-32}$$

where

$$F(\beta) = \frac{\omega\mu}{2\beta} J_0 \frac{e^{-j\beta(x-x')} + 2\cos\beta(x+x')\Gamma e^{-j2\beta l} + \Gamma^2 e^{-j4\beta l} e^{j\beta(x-x')}}{1-\Gamma^2 e^{-j4\beta l}} \frac{e^{-j\sqrt{k_0^2-\beta^2}z}}{\sqrt{k_0^2-\beta^2}} \tag{2-33}$$

The integration path in the complex β plane lies around branch cut $\kappa = \sqrt{k_0^2 - \beta^2}$, as shown in Figure 2-2. The branch points are at $\beta = \pm k_0$, the poles are located at $\beta = 0$ and $\beta = \frac{n\pi}{2d} + j\frac{n\lambda}{4d^2\sqrt{\varepsilon_w - 1}}$ for the TE polarization.

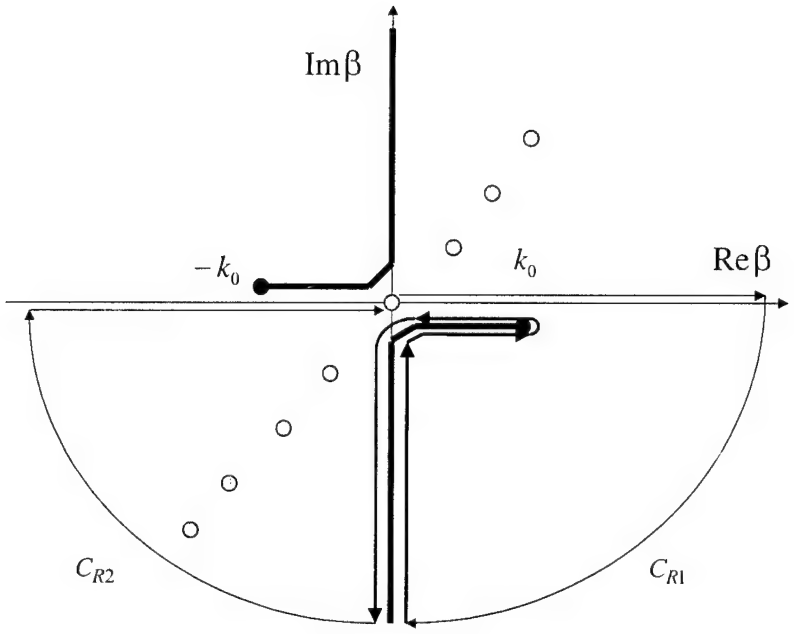

Figure 2-2 Integration Path in complex β plane

By Cauchy's residue theorem, the contour around the branch cut may be deformed into the real β axis by summing the residues of the poles crossed in the deformation. If C_{R1} and C_{R2} are two segments of the contour for $R \to \infty$, it is easily shown that the integration over C_{R1} and C_{R2} vanish. Thus

$$\int_C F(\beta)d\beta = 2\pi j \sum_{\beta_n} \text{res}\{F(\beta)\} - \int_{-\infty}^{\infty} F(\beta)d\beta \qquad (2\text{-}34)$$

Since $F(\beta)$ is odd function,

$$\int_{-\infty}^{\infty} F(\beta)d\beta = 0 \tag{2-35}$$

Because the only contribution in (2-34) comes from the residues in β plane.

We have

$$E_y(x,z) = -\frac{\omega\mu_0}{2d} J_0 \left(\sum_{n=even} \sin(\beta_n x)\sin(\beta_n x') \frac{e^{-j\sqrt{k_0^2-\beta_n^2}z}}{\sqrt{k_0^2-\beta_n^2}} + \sum_{n=odd} \cos(\beta_n x)\cos(\beta_n x') \frac{e^{-j\sqrt{k_0^2-\beta_n^2}z}}{\sqrt{k_0^2-\beta_n^2}} \right) \tag{2-36}$$

2.4 Modal Fields for TM Polarization in a 2-D Tunnel

By the principle of duality, we can find the magnetic modal fields in 2-D tunnel for excitation by a magnetic line source. The solution is found from (2-36) by replacing μ_0 by ε_0. Thus

$$H_y(x,z)=\frac{\omega\varepsilon_0}{2d}M_0\left(\sum_{n=even}\sin(\beta_n x)\sin(\beta_n x')\frac{e^{-j\sqrt{k_0^2-\beta_n^2}z}}{\sqrt{k_0^2-\beta_n^2}}+\sum_{n=odd}\cos(\beta_n x)\cos(\beta_n x')\frac{e^{-j\sqrt{k_0^2-\beta_n^2}z}}{\sqrt{k_0^2-\beta_n^2}}\right) \tag{2-37}$$

However the wavenumvers β_n must be found accounting for the TM reflection coefficient given by

$$\Gamma^{TM}=-\frac{\frac{\beta_w}{\omega\varepsilon_0\varepsilon_w}-\frac{\beta}{\omega\varepsilon_0\varepsilon_w}}{\frac{\beta_w}{\omega\varepsilon_0\varepsilon_w}+\frac{\beta}{\omega\varepsilon_0\varepsilon_w}}=\frac{\varepsilon_w\beta-\beta_w}{\varepsilon_w\beta+\beta_w} \tag{2-38}$$

The first two terms of the Taylor series expansion of Γ^{TM} about $\delta=0$ give

$$\Gamma^{TM}=\Gamma^{TM}(\delta=0)+\delta\frac{2\varepsilon_w\left(\beta^2-\beta_w^2\right)}{\beta_w(\varepsilon_w\beta+\beta_w)^2} \tag{2-39}$$

Making the same approximations that lead to the expression (2-28) for β_n in the case of TE polarization, we find that

$$\beta_n=\frac{n\pi}{2d}+j\frac{n\varepsilon_w\lambda}{4d^2\sqrt{\varepsilon_w-1}} \tag{2-40}$$

2.5 Mode Attenuation in 2-D Tunnels

Many propagating modes exist in tunnel when the operating frequency is high. Because each mode has different attenuation constant, only lower modes are important for long tunnels. The attenuation constant for a TE mode is defined by

$$\alpha^{TE}(dB/m) = 20\log\left(e^{\mathrm{Im}(\kappa_n)}\right) \tag{2-41}$$

$$\alpha^{TE}(dB/m) = \frac{20\,\mathrm{Im}(\kappa_n)}{\ln 10} = \frac{20}{\ln 10}\left[\frac{n^2}{2\sqrt{\varepsilon_w - 1}}\left(\frac{\lambda^2}{w^3}\right)\right] = \frac{10}{\ln 10}\frac{n^2}{\sqrt{\varepsilon_w - 1}}\gamma \tag{2-42}$$

where the parameter γ is defined by

$$\gamma = \frac{\lambda^2}{(2d)^3} \tag{2-43}$$

From equation (2-42), we observe that the mode attenuation is dependent on the factor $\frac{\lambda^2}{(2d)^3}$ and the square of mode index number. That means that the lower modes are dominant far from the transmitter, and that narrow tunnels have higher attenuation than wide tunnels for given operating frequency. Similarly, we can define the TM mode attenuation constant as

$$\alpha^{TM}(dB) = \frac{10}{\ln 10}\frac{\varepsilon_w n^2}{\sqrt{\varepsilon_w - 1}}\gamma \tag{2-44}$$

In figure 2-3 we have plotted the attenuation constant for the dominant n=1 mode versus tunnel dimension and wavelength assuming $\varepsilon_w = 6$. For example, a 450 MHz radio wave propagating in a 4 m wide tunnel has γ=0.0069, so that the attenuation of dominant TE mode is 1.349 dB per 100 m. For the n=2 mode, the attenuation constant is

5.395 dB per 100 m, while for n=3, 4 the attenuation constant is 12.139 dB, 21.58 dB per 100 m, respectively. Hence only a few lowest modes contribute the received power far from the transmitter.

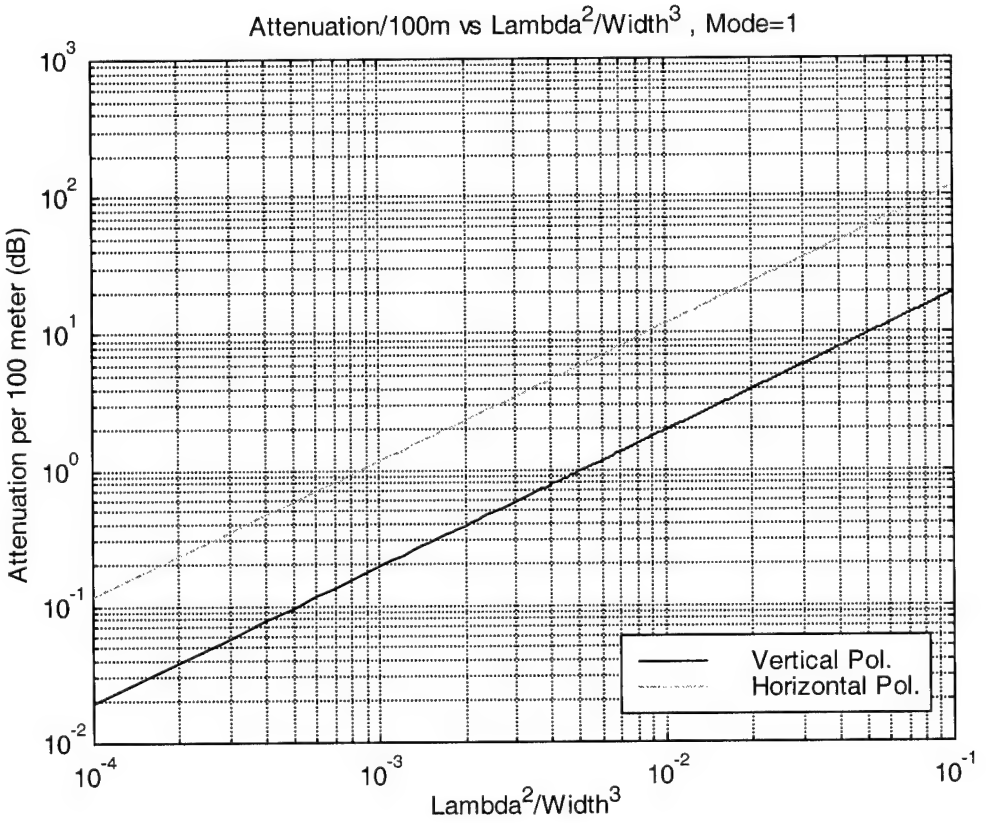

Figure 2-3 Attenuation constant versus tunnel dimension and frequency through the parameter $\frac{\lambda^2}{(2d)^3}$

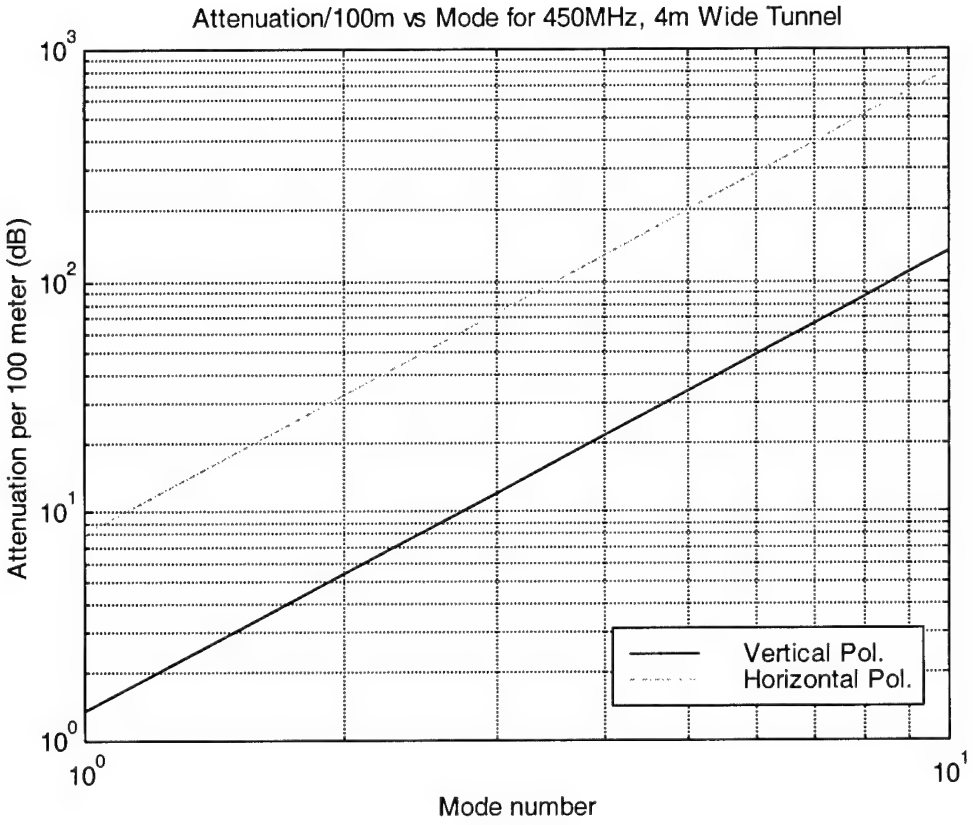

Figure 2-4 Attenuation constant versus mode number

2.6 Fields in a 2-D Tunnel for Point Source Excitation

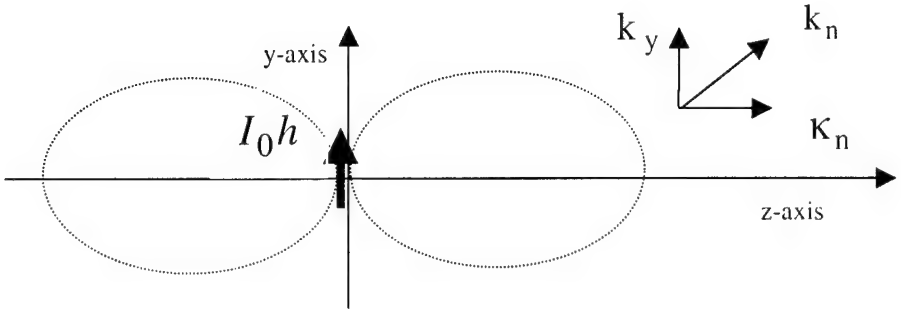

Figure 2-5 Point Source radiation in y-z plane

We have previously derived the modal expressions of the fields excited by a line source. We need to modify the expressions for excitation by a small dipole (point source). To do this, we first consider the dipole to be constructed from a spectrum of phased line sources of strength $\frac{I_0 h}{2\pi}$ with wavenumber k_y, as suggested in Figure 2-5. Thus the y variation of the dipole is

$$I_0 h\delta(y) = I_0 h \frac{1}{2\pi}\int_{-\infty}^{\infty} e^{-jk_y y} dk_y \tag{2-45}$$

Now suppose that the modal fields E_y for the phased line source of unit amplitude is written in the form

$$E_y(x,y,z) = \sum_n A_n E_n(x) e^{-jk_y y} e^{-j\kappa_n z} \tag{2-46}$$

where A_n is the amplitude modal fields, $\kappa_n = \sqrt{k_n^2 - k_y^2}$ and k_n is wavenumber of mode in y-z plane. Then from (2-45) and (2-46), the electric field due to the point source is

$$E_y(x,y,z) = \frac{I_0 h}{2\pi}\int_{-\infty}^{\infty}\sum_n A_n E_n(x) e^{-jk_y y} e^{-j\kappa_n z} dk_y \tag{2-47}$$

When y is small component to z, primary contribution to the integral (2-47) comes from the vicinity of $k_y = 0$. In this case we can approximate κ_n as

$$\kappa_n = \sqrt{k_n^2 - k_y^2} \approx k_n - \frac{k_y^2}{2k_n} \tag{2-48}$$

Using (2-48), the integration in (2-47) is approximated as

$$E_y(x,y,z) \approx \frac{I_0 h}{2\pi}\int_{-\infty}^{\infty}\sum_n A_n E_n(x) e^{-jk_y y} e^{-j\left(k_n - \frac{k_y^2}{2k_n}\right)z} dk_y \tag{2-49}$$

At large distance down a tunnel, the height y of the observation point will be about to the same as that of source, so that we may set dipole y = 0 in (2-47) to obtain

$$E_y(x,z) \approx \frac{I_0 h}{2\pi}\sum_n A_n E_n(x) e^{-jk_n z}\int_{-\infty}^{\infty} e^{j\frac{k_y^2}{2k_n}z} dk_y \tag{2-50}$$

The integration of (2-50), can be evaluated explicitly as

$$\int_{-\infty}^{\infty} e^{j\frac{k_y^2}{2k_n}z} dk_y = \sqrt{\frac{j2k_n}{z}}\int_{-\infty}^{\infty} e^{-u^2} du = \sqrt{\frac{j2k_n}{z}}\sqrt{\pi} \tag{2-51}$$

Hence we have the modal field from the point source at $y = 0$,

$$E_y(x,z) \approx \frac{I_0 h\sqrt{\kappa_n}}{\sqrt{2\pi z}} e^{j\frac{\pi}{4}} \sum_n A_n \mathrm{E}_n(x) e^{-j\kappa_n z} \tag{2-52}$$

For the TE polarization, the modal fields sum is given by

$$\sum_n A_n \mathrm{E}_n(x) e^{-j\kappa_n z} = -\frac{\omega\mu_0}{2d}\left[\sum_{n=even} \sin(\beta_n x)\sin(\beta_n x')\frac{e^{-j\kappa_n z}}{\kappa_n} + \sum_{n=odd} \cos(\beta_n x)\cos(\beta_n x')\frac{e^{-j\kappa_n z}}{\kappa_n}\right] \tag{2-53}$$

With the help of (2-52) and (2-53), the electric field at the receiver point due to a dipole is

$$E_y(x,z) = -e^{j\frac{\pi}{4}} \frac{I_0 h\sqrt{\kappa_n}}{\sqrt{2\pi z}} \frac{\omega\mu_0}{2d}\left[\sum_{n=even} \sin(\beta_n x)\sin(\beta_n x')\frac{e^{-j\kappa_n z}}{\kappa_n} + \sum_{n=odd} \cos(\beta_n x)\cos(\beta_n x')\frac{e^{-j\kappa_n z}}{\kappa_n}\right] \tag{2-54}$$

where $\kappa_n = \sqrt{k_0{}^2 - \beta_n{}^2}$ and $\beta_n = \frac{n\pi}{2d} + j\frac{n\lambda}{4d^2\sqrt{\varepsilon_r - 1}}$ for TE mode

For convenience in evaluating the communication channel, it is desirable to express the results in terms of path loss between isotropic antennas, or its reciprocal called the path gain. In order to make this interpretation, recognize that the power radiation by the Hertzian dipole is

$$P_T = \frac{1}{2} R_r I^2 = \frac{1}{2} I^2 \left(\frac{2\pi}{3}\eta\left(\frac{h}{\lambda}\right)^2\right) = 40\frac{\pi^2}{\lambda^2}(I \cdot h)^2 \tag{2-55}$$

where $\eta = 120\pi$ is the impedance of free space. The effective power radiated by the dipole in z direction $P_{ERP} = G_d P_T$ where the antenna gain G_d for a Hertzian dipole $= \frac{3}{2}$. Thus the equivalent amplitude of the dipole is

$$40\frac{\pi^2}{\lambda^2}(I_0 \cdot h)^2 = \frac{P_{ERP}}{G_d} \tag{2-56}$$

Using (2-55) and (2-56) the dipole current amplitude equivalent to radiation of P_{ERP} watts by an isotropic source is

$$I_0 \cdot h = \left(\frac{\lambda}{\pi}\right)\sqrt{\frac{P_{ERP}}{40G_d}} \tag{2-57}$$

If the effective radiated power is $P_{ERP} = 1$ Watt, then

$$I_0 \cdot h = \left(\frac{\lambda}{\pi}\right)\sqrt{\frac{1}{60}} \tag{2-58}$$

The modal fields for $P_{ERP} = 1$ Watt Hertzian dipole is therefore given by

$$E_y(x,z) = -e^{j\frac{\pi}{4}}\frac{\omega\mu_0}{\sqrt{120\pi z}}\left(\frac{\lambda}{2\pi d}\right)\left[\sum_{n=even}\sin(\beta_n x)\sin(\beta_n x')\frac{e^{-j\kappa_n z}}{\sqrt{\kappa_n}} + \sum_{n=odd}\cos(\beta_n x)\cos(\beta_n x')\frac{e^{-j\kappa_n z}}{\sqrt{\kappa_n}}\right] \tag{2-59}$$

where $\beta_n = \frac{n\pi}{2d} + j\frac{n\lambda}{(2d)^2\sqrt{\varepsilon_w - 1}}$ for Vertical Polarization.

The power received by a point source can be expressed in terms of the field at the receiver via

$$P_{RX} = G_{RX}\left(\frac{\lambda^2}{4\pi}\right)\frac{|E(x,z)|^2}{2\eta} \tag{2-60}$$

For an isotropic receiver, G_{RX} =1, substituting (2-59) into (2-60) gives the received power for P_{ERP}=1 Watt, which is equivalent to the Path Gain for the radio link (path gain is the inverse of the path loss).

In Figure 2-6 and 2-7, we have plotted the path gain as a function of distance between isotropic antennas for propagation of a 4 m wide 2-D tunnel at frequency ranging from 30 MHz to 1.8 GHz. The dielectric constant of side walls is taken to be $\varepsilon_r = 6$ and the conductivity $\sigma = 0.01$. The Path Gain is averaged over the width of the tunnel and normalized to the received power at 10 m from the transmitter. At small separation, the path gain is nearly that of free space, which for isotropic antenna as at 10 m separation is $\left(\frac{\lambda}{40\pi}\right)^2$. In Figure 2-6, the antenna polarization is vertical and transmitter is located at the mouth of tunnel and 2 m from the tunnel side wall. Because of the narrow width of the tunnel, at 100 MHz and below the signal decreases rapidly with distance. The path gain for horizontal polarization of the antenna is shown in Figure 2-7. Because the attenuation constant of the TM (Horizontal Polarization) modes is greater than for TE (Vertical Polarization) modes for given tunnel width, we see that the signal decreases more rapidly for horizontal polarization than for vertical polarization.

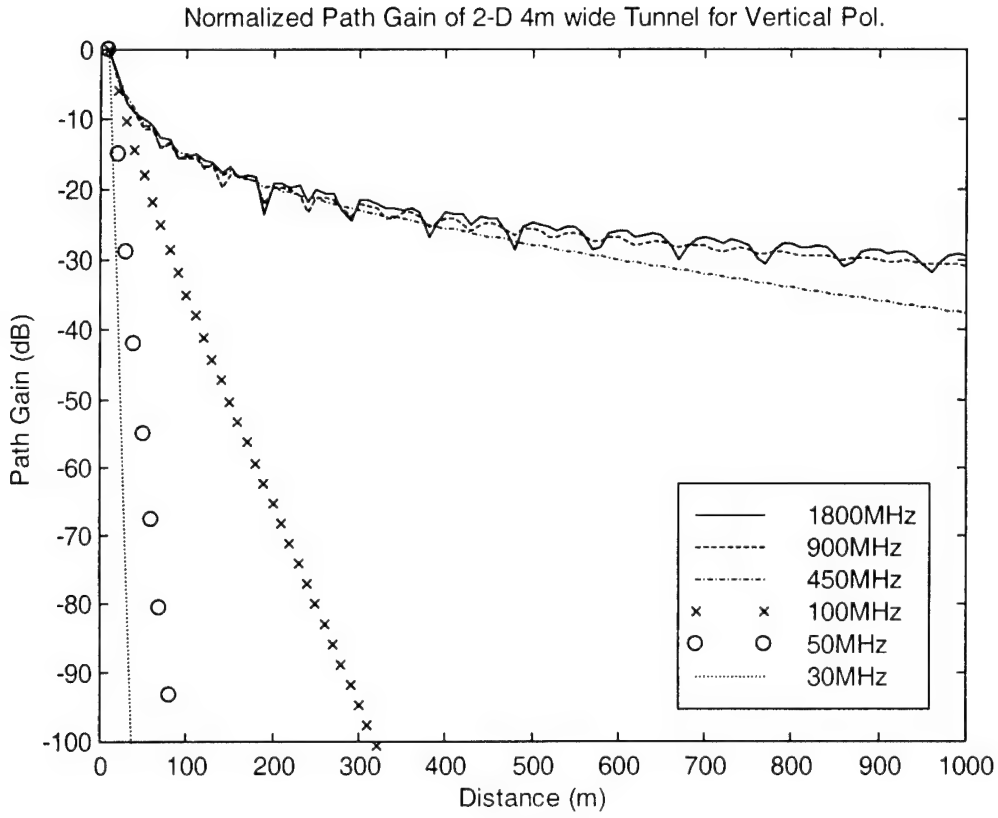

Figure 2-6 Normalized Path Gain of the 4m wide 2-D Tunnel for various frequencies

Vertical Polarization (ε_r=6, σ = 0.01)

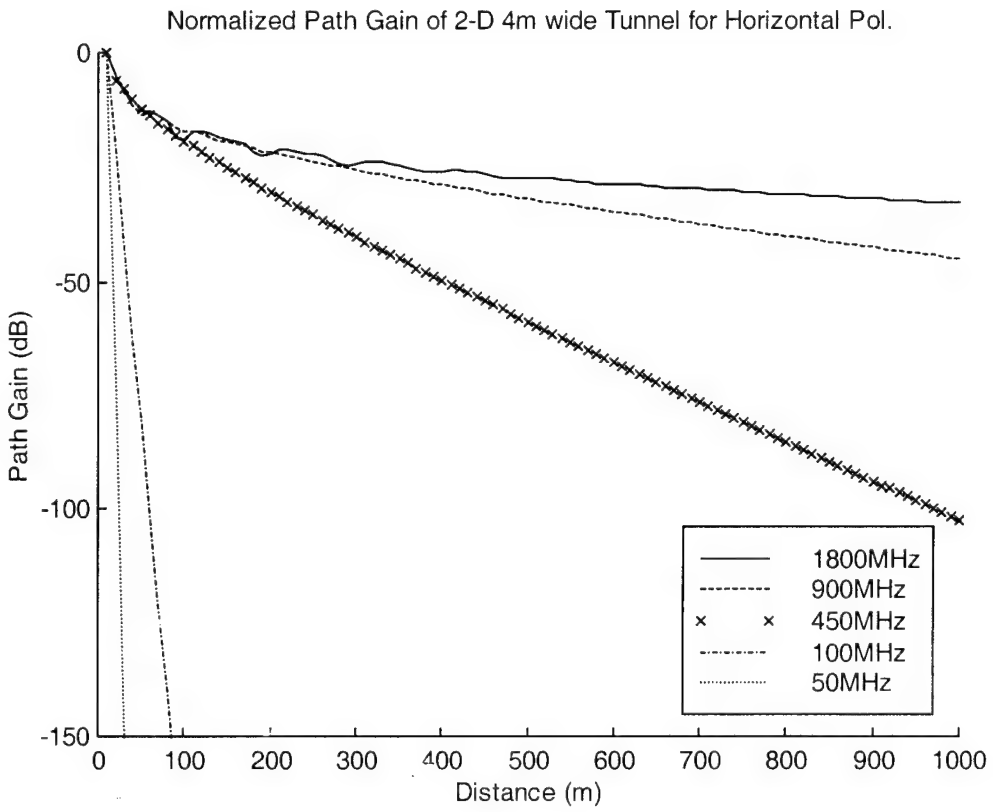

Figure 2-7 Normalized Path Gain of the 4m wide 2-D Tunnel for various frequencies

Horizontal Polarization (ε_r=6, $\sigma = 0.01$)

3. Mode Coupling at L, T, and Cross Junctions

3.1 Mode diffraction analysis of coupling

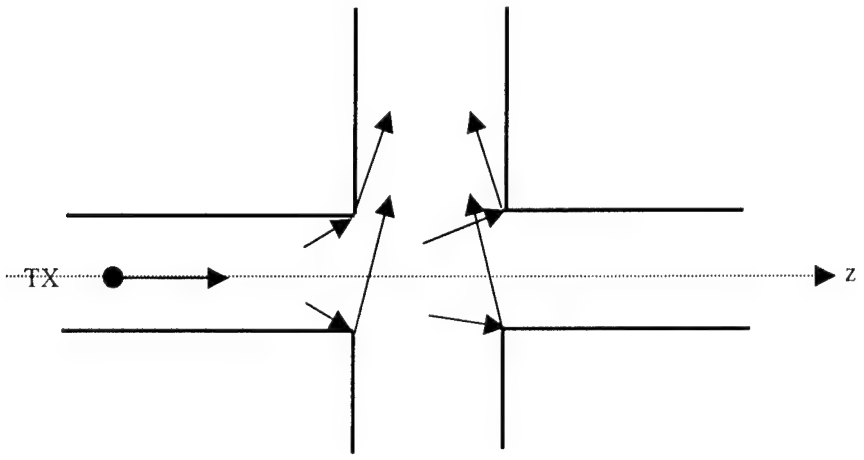

Figure 3-1 Propagation in 2-D Cross Junction Tunnel

In order to illustrate the approach used here to couple into side tunnels, consider a source located in one arm of a cross junction of a 2-D tunnel, as shown in Figure 3-1. Since $k_0 d >> 1$, the modes excited by the source in the left arm will propagate to the gap and couple with little attenuation into right arm. They will also couple into the upper and lower arms as a result of the illumination in the aperture of the arms. As a first approximation, the illumination in the aperture is given by $e^{-j\kappa_n z} = \cos(\kappa_n z) + j\sin(\kappa_n z)$. For the lower modes in the left arm, κ_n is close to k_0, and hence is much larger than the transverse wavenumber β_n of those modes. As seen in the cross arms, the wave number κ_n in the aperture corresponds to the transverse wavenumber β_n in the cross arm. Thus, the aperture fields excite only the very high order modes in the lower and upper arms that have transverse wavenumber β_n close to

k_0. Since these modes have very high loss, they cannot contribute to the fields at significant distances along the upper and lower arms.

In view of the foregoing argument, coupling to low modes must occur through a different mechanism. Felsen, in studying reflection of modes incident on the open end of a waveguide, suggested such a mechanism [9]. Viewing the incident modes as composed of multiply reflected plane waves, the coupling to the reflected modes resulted from diffraction at the edges of the open end waveguide. Each plane wave excites diffracted rays that are multiply reflected in the waveguide walls. By summing the diffracted ray contributions and using the Poisson sum formula, it is possible to translate the diffracted rays into a modal sum, with the amplitude of the modes given by the diffraction coefficient evaluated at the mode angle. The diffracting corners and the rays that excite the cross tunnel are shown in Figure 3-1. This approach is especially will suited to the case when $k_0 d >> 1$, as we have found necessary for propagation over a significant distance in a tunnel. The multiply reflected rays originating at the upper right hand corner of the upper arm in Figure 3-1 are shown Figure 3-2. In this figure we have reoriented the coordinate system so that z lies along the axis of the cross tunnel.

The field received at a distance z along the tunnel is the sum of the fields carried by the multiply reflected ray produced by diffraction at the corners of the tunnel. The multiply reflected rays arriving at the receiver may be viewed as coming from multiple images of the edges in the tunnel walls. The image array for a single line source at the right hand edge is shown in Figure 3-2. Similarly, the left hand edge gives the diffracted ray contributions that appear to come from the images shown in Figure 3-3.

Each mode incident on the junction will generate a set of sources of the type shown in Figure 3-2 and Figure 3-3. The source corresponding to the right hand edge will have strength u_0 that is determined by the phase and amplitude of the incident modal field, and a pattern function $D(\theta_n, \theta_{in})$. Here θ_{in} is the angle of incident plane wave comprising the mode incident on the junction, and θ_n is the angle of the diffracted ray. Similarly, the left hand edge will have amplitude u_1 and pattern function $D(\theta_n, \theta_{in})$. The explicit expression for u_0, u_1 and $D(\theta_n, \theta_{in})$ will be discussed later. When u_0, u_1 and

$D(\theta_n, \theta_{in})$ are known, then for TE polarization the field E_y at the receiver location (x,z) is given by

$$E_y(x,z) = \sum_{i=0,1} \sum_{n=-\infty}^{\infty} u_i \Gamma(\theta_n)^p D(\theta_n, \theta_{in}) \frac{e^{-jk_0 r_n}}{\sqrt{r_n}} \tag{3-1}$$

$$r_n = \sqrt{z^2 + (x - (4n \pm 1)d)^2} \tag{3-2}$$

$$\theta_n = \tan^{-1}\left(\frac{|x - (4n \pm 1)d|}{z} \right) \tag{3-3}$$

where the + sign is applies the right hand edge (i=0), the – sign is for the left hand edge (i=1). In (3-1) ~ (3-3), n=0 refers to the direct ray and $n = \pm 1, \pm 2, \pm 3, \ldots$ refers to rays coming from the images, as indicated in Figure 3-2 and 3-3. The index $p \geq 0$ gives the number of reflections undergone by the ray corresponding to the particular image. The values of p are listed in Figure 3-2 and 3-3, and expression for p in terms of n will be given in the subsequent discussion.

In the case of a waveguide with metallic walls, $|\Gamma| = 1$ so that only the sign of $(\Gamma)^p$ needs to be accounted for. In the case of dielectric waveguide walls, $(\Gamma)^p$ is a function of the number of reflections through the glancing angle θ_n, and through the exponent p. In order to generalizing Felsen's method to the case of dielectric walls, it is necessary to consider $[p(\theta_n)]^p$ as a function of ray direction so that the pattern function of source becomes $[\Gamma(\theta_n)]^p D(\theta_n, \theta_{in})$. In this way the field from each image accounts for the multiple reflection.

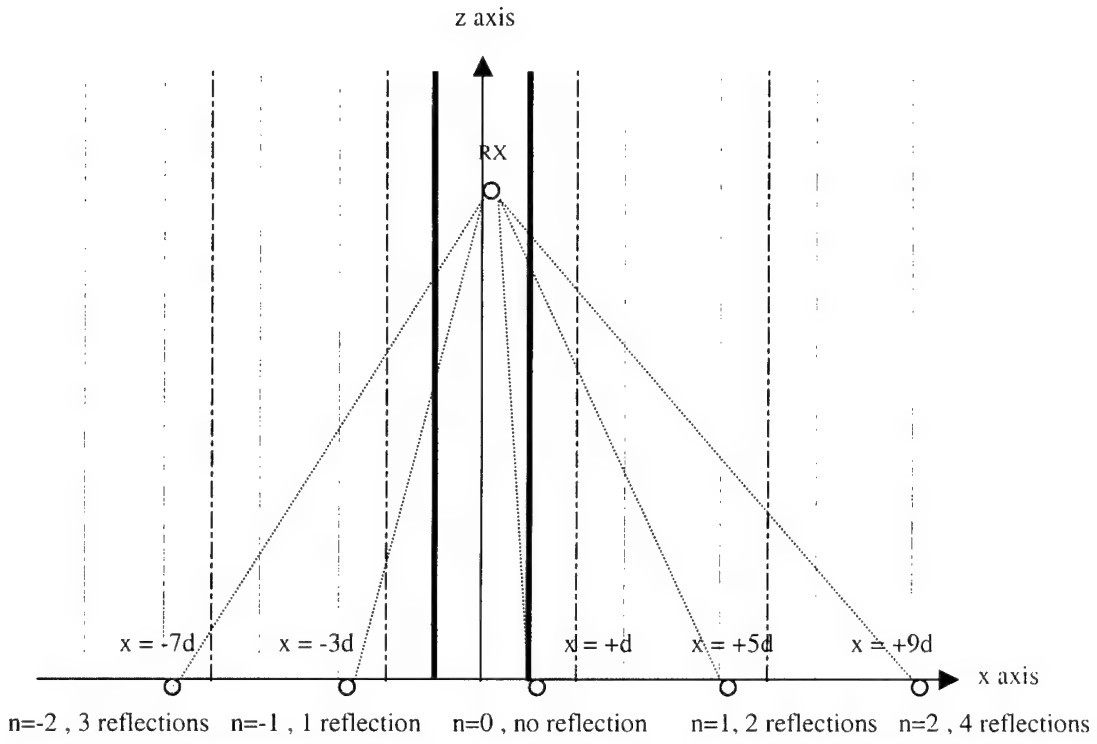

Figure 3-2 Diffracted rays due to the images of the line source at the right hand edge

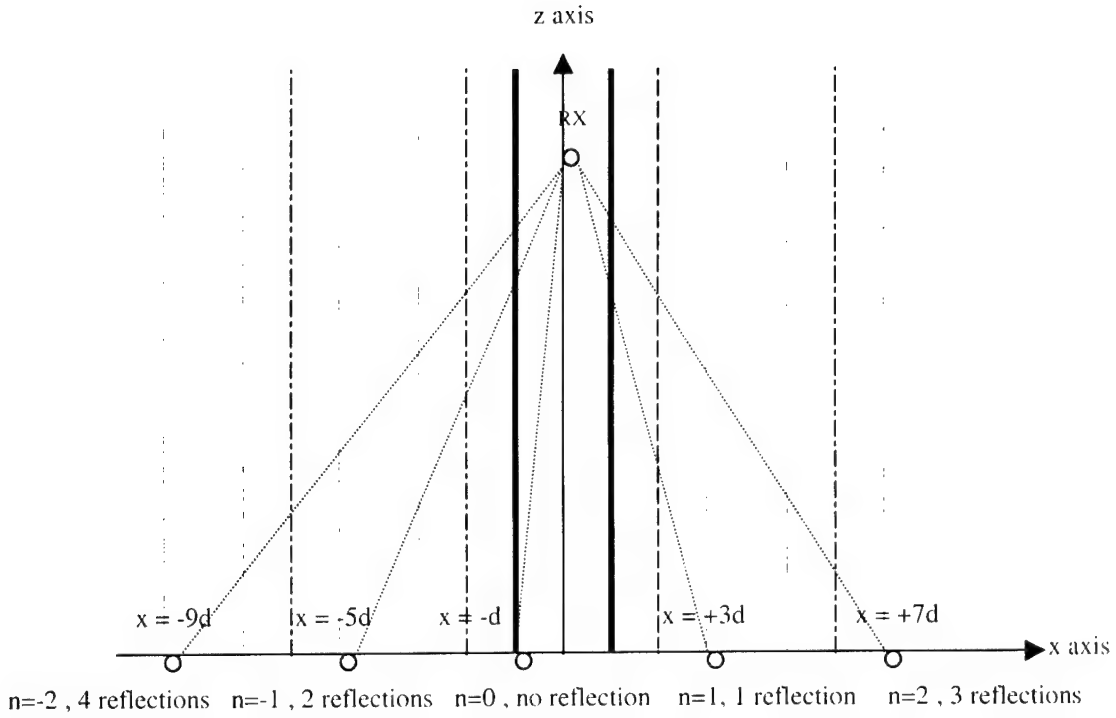

Figure 3-3 Diffracted rays due to the images of the line source at the left hand edge

3-2 Ray-Mode conversion

For propagation over a significant distance along the tunnel, many reflections must be accounted for in the sum (3-1). A more convenient representation of the field in this case is found by converting the ray sum into mode sum, as discussed below in terms of Poisson sum formula [10].

A periodic function $\tilde{f}(x)$ with period 4d can be represented in form

$$\tilde{f}(x) = \sum_{n=-\infty}^{\infty} f(x+4nd) \tag{3-4}$$

where $f(x)$ is some function defined on the infinite interval. As applied to the waveguide problem $\tilde{f}(x)$ is the y component of electric field inside the waveguide $-d < x < d$, and is the analytic continuation of the field for the remainder of the period 4d ($-2d < x < -d$ and $d < x < 2d$). The Poisson sum formula expresses this function as the sum

$$\tilde{f}(x) = \frac{1}{4d} \sum_{m=-\infty}^{\infty} C_m e^{j\frac{m\pi}{2d}x} \tag{3-5}$$

where C_m is the Fourier transform of $f(x)$ given by

$$C_m = \int_{-\infty}^{\infty} f(x) e^{-j\frac{m\pi}{2d}x} dx \tag{3-6}$$

If the reflection coefficient $\Gamma = 1$, then we can interpret $f(x)$ as being the y component of the electric field due to a line source inside the waveguide, in which case the term $f(x+4nd)$ represents the field due to one of the images of the line source in the waveguide walls, as shown in Figure 3-2 for a line source at d, or in Figure 3-3 for a line

source at –d. When the waveguide walls are not perfectly reflecting, the definition of $f(x+4nd)$ is modified to include reflection coefficient, as discussed below.

By grouping terms in (3-5) for $m = \pm|m|$, the sum (3-5) is expressed in terms of the waveguide modes. Note that the m = 0 mode in the dielectric waveguide would be highly attenuated and is ignored here. According to Poisson sum formula, the total field $E_y(x,z)$ in the waveguide is given by the modal expression

$$E_y(x,z) = \frac{1}{2d}\left[\sum_{m=1}^{\infty} \frac{C_m + C_{-m}}{2} \cos\left(\frac{m\pi}{2d}x\right) + j\sum_{m=1}^{\infty} \frac{C_m - C_{-m}}{2} \sin\left(\frac{m\pi}{2d}x\right)\right] \tag{3-7}$$

The coefficient C_m is given by the Fourier transform of an equivalent line source field $f(x)$.

3.2.1 Evaluation of C_m for diffraction at the left hand corner

The choice of the equivalent line source field can be understood in terms of Figure 3-3, where we have shown the original line source at –d and its images at +3d, +7d, … and –5d, -9d, … . The images on the right are indexed by n = 1, 2, 3, … and those on the left by n = -1, -2, -3, … . Each image represents the ray that is reflected p times in the waveguide walls, where p = 2n-1 for n>0 and p = -2n for n<0. The individual terms in the ray sum (3-4), which represent the multiply reflected rays, will have the values

$$f(x+4nd) = u_1[\Gamma(\theta_n)]^p D(\theta_n, \theta_{in}) \frac{e^{-jk_0 r_n}}{\sqrt{r_n}} \tag{3-8}$$

where

$$r_n = \sqrt{z^2 + \{(x+d) - 4nd\}^2} \tag{3-9}$$

and

$$\theta_n = \tan^{-1}\left[\frac{|(x+d) - 4nd|}{z}\right] \tag{3-10}$$

Here u_1 is the amplitude of the field incident on the edge and the diffraction coefficient $D(\theta_n, \theta_{in})$ gives the pattern function of the line source.

By replacing x+4nd in (3-8) ~ (3-10) by x, it is seen that

$$f(x) = u_1[\Gamma(\theta)]^{p(x)} D(\theta_n, \theta_{in}) \frac{e^{-jk_0 r}}{\sqrt{r}} \tag{3-11}$$

where

$$r = \sqrt{z^2 + (x+d)^2} \tag{3-12}$$

and

$$\theta = \tan^{-1}\left(\frac{|x+d|}{z}\right) \tag{3-13}$$

In (3-11) the exponent of the reflection coefficient is shown by the step curve in Figure 3-4

In order to carry out the integration (3-6), we write $\Gamma^{p(x)}$ in the form

$$[\Gamma(\theta)]^{p(x)} = e^{p(x)\ln\Gamma(\theta)} \tag{3-14}$$

If we now express Γ as a function of θ and assume that z is large so that $|\sin\theta| << 1$ for the lower values of $|n|$, then for TE polarization we have

$$\Gamma(\theta) = \frac{\sin\theta - \sqrt{\varepsilon_w - \cos^2\theta}}{\sin\theta + \sqrt{\varepsilon_w - \cos^2\theta}} \approx -1 + \frac{2\sin\theta}{\sqrt{\varepsilon_w - 1}} \tag{3-15}$$

We further approximate $\ln\Gamma(\theta)$ as

$$\ln\Gamma(\theta) = j\pi + \ln\left[1 - \frac{2\sin\theta}{\sqrt{\varepsilon_w - 1}}\right] \approx j\pi - \frac{2|\sin\theta|}{\sqrt{\varepsilon_w - 1}} \tag{3-16}$$

Using the approximation in (3-14) gives

$$[\Gamma(\theta)]^{p(x)} = \exp\left[p(x)\left(j\pi - \frac{2\sin\theta}{\sqrt{\varepsilon_w - 1}}\right)\right] = (-1)^{p(x)} \exp\left[\frac{-2\sin\theta}{\sqrt{\varepsilon_w - 1}}\, p(x)\right] = -\mathrm{sgn}(x - 2d)\exp\left[\frac{-2\sin\theta}{\sqrt{\varepsilon_w - 1}}\, p(x)\right] \tag{3-17}$$

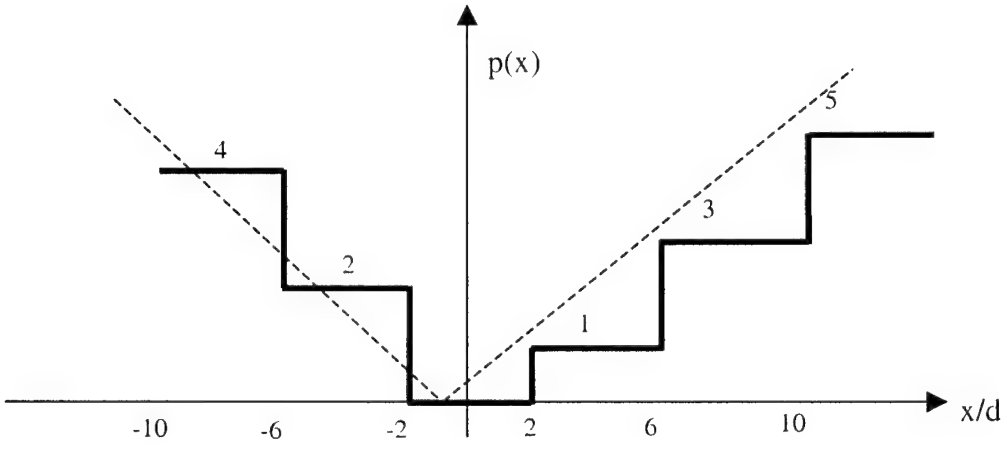

Figure 3-4 Variation of the reflection coefficient index $p(x)$ for the left hand edge

Note that (3-17) is a generalization of the approach used by Felsen [9] for metallic waveguides where $\Gamma = -1$ so that $\Gamma^{p(x)} = -\mathrm{sgn}(x-2d)$. Using (3-11) and (3-14) it is seen

$$C_m = -\int_{-\infty}^{\infty} u_1 D(\theta,\theta_{in})\,\mathrm{sgn}(x-2d)\exp\left[\frac{-2\sin\theta}{\sqrt{\varepsilon_w - 1}}\,p(x)\right]\frac{e^{-jk_0\sqrt{z^2+(x+d)^2}}}{\left\{z^2+(x+d)^2\right\}^{1/4}}\,e^{-j\frac{m\pi}{2d}x}\,dx \tag{3-18}$$

The function $\exp\left[\frac{-2\sin\theta}{\sqrt{\varepsilon_w - 1}}\,p(x)\right]$ in (3-18) has discontinuities due to the definition of $p(x)$ at x = $\pm$ 2d, $\pm$ 4d, $\pm$ 6d, ... However, since $|\theta|$ is small for $z >> d$, at the discontinuities closest to d, the jump in the exponent will be small. For discontinuities further from d, the exponential is already small so that it will give small contribution to the integration. We therefore approximate $p(x)$ in (3-18) by the ramp function $p(x) = \frac{|x+d|}{2d}$. This approximation is shown by the dashed lines in the Figure 3-4. The choice of this ramp function is made to in order to simplify the asymptotic evaluation of the integration for C_m. The variation of the term $\exp\left[\frac{-2\sin\theta}{\sqrt{\varepsilon_w - 1}}\,p(x)\right]$ in (3-18) using the exact and approximate forms of $p(x)$ are plotted in Figure 3-5. In (3-18) $\sin\theta = \frac{(x+d)}{\sqrt{z^2+(x+d)^2}}$.

Using the foregoing expressions and the approximation form for $p(x)$, we define the functions

$$q(x) = k_0\sqrt{z^2+(x+d)^2} + \frac{m\pi}{2d}x - j\frac{(x+d)^2}{d\sqrt{\varepsilon_w - 1}\sqrt{z^2+(x+d)^2}} \tag{3-19}$$

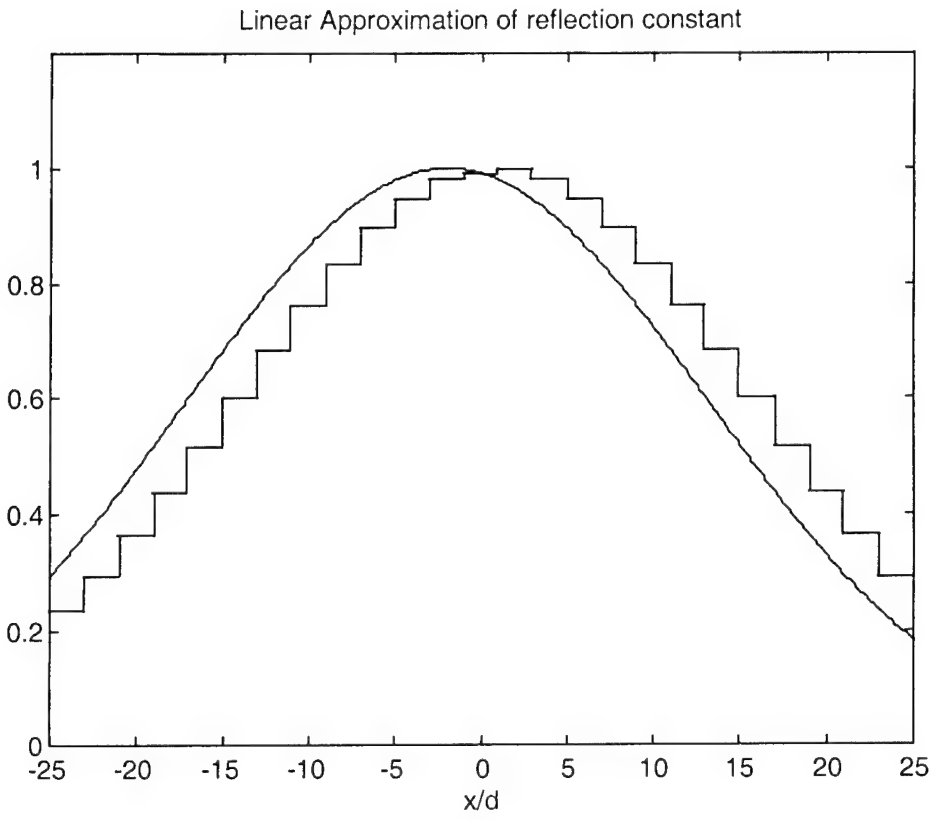

Figure 3-5 Linear approximation of reflection constant $\exp\left(\frac{-2\sin\theta}{\sqrt{\varepsilon_w - 1}}p(x)\right)$ for the diffraction of left hand edge, where θ is given by (3-13), z = 100 m and d = 2 m

$$g(x) = \frac{D(\theta, \theta_{in})}{\left\{z^2 + (x+d)^2\right\}^{1/4}} \tag{3-20}$$

Then

$$C_m = -\int_{-\infty}^{\infty} u_1 \operatorname{sgn}(x-2d) g(x) e^{-jq(x)} dx \tag{3-21}$$

To simplify the integration we change variable to $\eta = x + d$, in which case

$$q(\eta) = k_0\sqrt{z^2+\eta^2} + \frac{m\pi}{2d}(\eta - d) - j\frac{\eta^2}{d\sqrt{\varepsilon_w - 1}\sqrt{z^2+\eta^2}} \tag{3-22}$$

$$g(\eta) = \frac{D(\theta, \theta_{in})}{\left\{z^2+\eta^2\right\}^{1/4}} \tag{3-23}$$

and

$$C_m = -\int_{-\infty}^{\infty} u_1 \operatorname{sgn}(\eta - 3d) g(\eta) e^{-jq(\eta)} d\eta \tag{3-24}$$

3.2.1.a Evaluation for m<0

For $m < 0$ and for $z >> d^2/\lambda$, the saddle point of $g(\eta)$ will lie in the region $\eta > 3d$. Then the integration can then be written in a form that allows the separate evaluation of the saddle point and end point contributions. This form is

$$C_m = -u_1\left\{\int_{-\infty}^{\infty} g(\eta) e^{-jq(\eta)} dx - 2\int_{-\infty}^{3d} g(\eta) e^{-jq(\eta)} d\eta\right\} \tag{3-25}$$

For the region of interest $z >> d >> \lambda$, the saddle point η_s is obtained from the solution of $q'(\eta) = 0$. The derivation of $q(\eta)$ can be approximated by

$$q'(\eta) \approx \frac{k_0\eta}{z} + \frac{m\pi}{2d} - j\frac{2\eta}{dz\sqrt{\varepsilon_w - 1}} \tag{3-26}$$

and the saddle point is

$$\eta_s \approx -\frac{m\lambda}{4d} z - j\frac{m\pi}{d^2 k_0{}^2 \sqrt{\varepsilon_w - 1}} z \tag{3-27}$$

It is seen from (3-27) that for m<0 and $z >> d^2/\lambda$, the value of $\mathrm{Re}\,\eta_s$ will be greater than 3d.

Consistent with the foregoing approximation we find that $q(\eta_s)$, $g(\eta_s)$ and $q''(\eta_s)$ are given by

$$q(\eta_s) \approx k_0 \sqrt{z^2 + \eta_s{}^2} + \frac{m\pi}{2d}\eta_s - \frac{m\pi}{2} - j\frac{\eta_s{}^2}{zd\sqrt{\varepsilon_w - 1}}$$

$$\approx \left\{ k_0 - \frac{m\pi}{2d}\left(\frac{m\lambda}{4d} + j\frac{m\pi}{d^2 k_0{}^2 \sqrt{\varepsilon_w - 1}} \right) \right\} z - \frac{m\pi}{2} \tag{3-28}$$

$$g(\eta_s) = \frac{D(\theta_s, \theta_{in})}{\left\{ z^2 + \eta^2 \right\}^{1/4}} \approx \frac{D(\theta_m, \theta_{in})}{\sqrt{z}} \tag{3-29}$$

where

$$\theta_m = \tan^{-1}\left(\frac{|\eta_s|}{z} \right) \approx \tan^{-1}\left(\frac{|m|\lambda}{4d} \right) \tag{3-30}$$

and

$$q''(\eta_s) \approx \frac{k_0}{z} \tag{3-31}$$

The saddle point integration [11] for C_m with m<0 is obtained as

$$\int_{-\infty}^{\infty} g(\eta)e^{-jq(\eta)}d\eta \approx \sqrt{\frac{2\pi}{jq''(\eta_s)}}g(\eta_s)e^{-jq(\eta_s)}$$

$$= \sqrt{\frac{2\pi}{jk_0}}D(\theta_m,\theta_{in})e^{-j\left\{k_0-\frac{m\pi}{2d}\left(\frac{m\lambda}{4d}+j\frac{m\pi}{d^2k_0^2\sqrt{\varepsilon_w-1}}\right)\right\}z}e^{j\frac{m\pi}{2}}$$

$$\approx e^{-j\frac{\pi}{4}}\sqrt{\lambda}D(\theta_m,\theta_{in})e^{-j\kappa_m z}e^{j\frac{m\pi}{2}} \qquad (3\text{-}32)$$

Note that the coefficient of z in the exponent is the same as the value of κ_m given by (2-30A) for the mode solution in a straight tunnel under the condition that $d >> \lambda$.

The end point contribution to C_m is written in the form

$$I_{end} = \int_{-\infty}^{3d} g(\eta)e^{-jq(\eta)}d\eta \qquad (3\text{-}33)$$

If $z >> d^2/\lambda$, then the saddle point will be far from the end point and we can evaluate (3-33) asymptotically by approximating the exponent of integrand in (3-33) near the endpoint as

$$q(\eta) = q(3d) + (\eta - 3d)q'(3d) \qquad (3\text{-}34)$$

With the help of (3-34), the end point integration becomes

$$I_{end} \approx g(3d)e^{-jq(3d)}\int_{-\infty}^{3d} e^{-j(\eta-3d)q'(\eta)}d\eta \qquad (3\text{-}35)$$

Letting $\tau = j(\eta - 3d)q'(\eta)$, we have

$$\frac{g(3d)}{jq'(3d)}e^{-jq(3d)}\int_{\infty}^{0} e^{-\tau}d\tau = \frac{g(3d)}{jq'(3d)}e^{-jq(3d)} \qquad (3\text{-}36)$$

where

$$q(3d) \approx k_0 z + m\pi \tag{3-37}$$

$$q'(3d) \approx \frac{m\pi}{2d} \tag{3-38}$$

$$g(3d) = \frac{D\left(\tan^{-1}\frac{3d}{z}, \theta_{in}\right)}{\left(z^2 + 9d^2\right)^{\frac{1}{4}}} \approx \frac{D(0, \theta_{in})}{\sqrt{z}} \tag{3-39}$$

Thus the end point integration in C_m is obtained as

$$\int_{-\infty}^{3d} g(\eta) e^{-jq(\eta)} d\eta \approx \frac{2dD(0, \theta_{in})}{jm\pi\sqrt{z}} e^{-j(k_0 z + m\pi)} \tag{3-40}$$

With the results of (3-32) and (3-40), C_m for m <0 becomes

$$C_m \approx -u_1 \left\{ e^{-j\frac{\pi}{4}} \sqrt{\lambda} D(\theta_m, \theta_{in}) e^{j\frac{m\pi}{2}} e^{-j\kappa_m z} - (-1)^m \frac{4dD(0, \theta_{in})}{jm\pi\sqrt{z}} e^{-jk_0 z} \right\} \tag{3-41}$$

For $z >> d^2/\lambda$, then $d/\sqrt{z} << \lambda$ and the second term in (3-41) coming from the end point integration is small compared to the first term due to the saddle point. We therefore omit the end point term from later analysis.

3.2.1.b Evaluation for m>0

For $m > 0$ the saddle point lies in the region $\eta < 3d$, and we may write

$$C_m = u_1 \left\{ \int_{-\infty}^{\infty} g(\eta) e^{-jq(\eta)} dx - 2 \int_{3d}^{\infty} g(\eta) e^{-jq(\eta)} d\eta \right\} \tag{3-42}$$

The evaluation of saddle point contribution is like that for m<0, and leads to expression (3-32). Using approximation employed to evaluated (3-33), the end point contribution in (3-42) is the negative of (3-40), or

$$\int_{3d}^{\infty} g(\eta) e^{-jq(\eta)} d\eta \approx \frac{2dD(0,\theta_{in})}{-jm\pi\sqrt{z}} e^{-j(k_0 z - m\pi)} \tag{3-43}$$

Thus the integration C_m for m>0 is given by

$$C_m \approx u_1 \left\{ e^{-j\frac{\pi}{4}} \sqrt{\lambda} D(\theta_m, \theta_{in}) e^{j\frac{m\pi}{2}} e^{-jK_m z} + (-1)^m \frac{4dD(0,\theta_{in})}{jm\pi\sqrt{z}} e^{-jk_0 z} \right\} \tag{3-44}$$

The second term in (3-44), which came from the end point integration, is small compared to the first term provided $z >> d^2/\lambda$. As in the case of m<0, we neglect this term in later analysis.

3.2.1.c Total field due to diffraction at the left hand edge

From the result of (3-41) and (3-44), and neglecting the second term, the diffracted modal electric field for $z >> d^2/\lambda$ due to the u_1 incident field to the left edge in the tunnel is obtained as

$$E_y(x,z) = u_1 e^{j\frac{\pi}{4}} \frac{\sqrt{\lambda}}{2d} \left\{ \sum_{m=odd} (-1)^{\frac{m-1}{2}} D(\theta_m, \theta_{in}) \cos\left(\frac{m\pi}{2d} x\right) e^{-j\kappa_m z} \right.$$
$$\left. - \sum_{m=even} (-1)^{\frac{m}{2}} D(\theta_m, \theta_{in}) \sin\left(\frac{m\pi}{2d} x\right) e^{-j\kappa_m z} \right\} \qquad (3\text{-}45)$$

where κ_m is given by (2-30A). Expression (3-45) is in the form of a modal sum, as in (2-26), except that the transverse wavenumber β_m is replaced by $m\pi/2d$. However, since the imaginary part of the transverse wavenumber in (2-26) is very small for $d >> \lambda$, the transverse variation in (3-45) is nearly that of the modal field.

3.2.2 Evaluation of C_m for diffraction at the right hand corner

For the diffracted field due to the right hand edge shown in Figure 3-2, the field expression in tunnel is expressed as

$$f(x) = u_0[\Gamma(\theta)]^{p(x)} D(\theta_n, \theta_{in}) \frac{e^{-jk_0 r}}{\sqrt{r}} \tag{3-46}$$

Here u_0 is the amplitude of the incident field at the right hand edge,

$$r = \sqrt{z^2 + (x-d)^2} \tag{3-47}$$

and

$$\theta = \tan^{-1}\left(\frac{|x-d|}{z}\right) \tag{3-48}$$

The exponent of reflection coefficient $p(x)$ in (3-46) is shown in Figure 3-6. Using the same approximation (3-17) for Γ, the reflection coefficient in (3-46) becomes

$$[\Gamma(\theta)]^{p(x)} \approx \text{sgn}(x+2d)\exp\left[\frac{-2\sin\theta}{\sqrt{\varepsilon_w - 1}} p(x)\right] \tag{3-49}$$

With (3-46) and (3-49), C_m is given by

$$C_m = \int_{-\infty}^{\infty} u_0 \,\text{sgn}(x+2d) D(\theta, \theta_{in}) \exp\left[\frac{-2\sin\theta}{\sqrt{\varepsilon_w - 1}} p(x)\right] \frac{e^{-jk_0\sqrt{z^2+(x-d)^2}}}{\left\{z^2 + (x-d)^2\right\}^{1/4}} e^{-j\frac{m\pi}{2d}x} dx \tag{3-50}$$

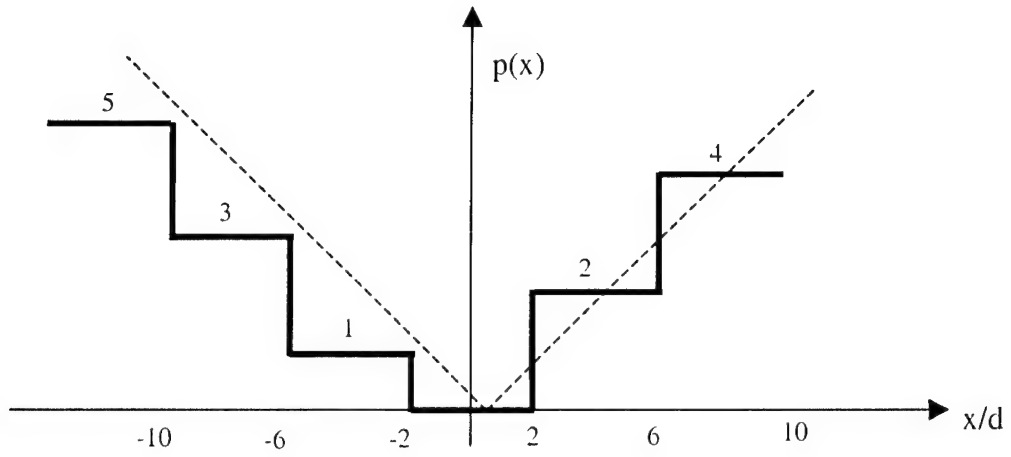

Figure 3-6 Variation of the reflection coefficient index $p(x)$ for right hand edge

As before, we approximate $p(x)$ in the exponent of (3-49) by the ramp function $p(x)=\frac{|x-d|}{2d}$ shown in Figure 3-6 to simplify the asymptotic integration. The integration for C_m is evaluated by same approaches as we showed for the diffraction of the left hand edge. Thus C_m for m>0 is obtained as

$$C_m \approx -u_0\left\{e^{-j\frac{\pi}{4}}\sqrt{\lambda}D(\theta_m,\theta_{in})e^{-j\frac{m\pi}{2}}e^{-jk_m z}+(-1)^m\frac{4dD(0,\theta_{in})}{jm\pi\sqrt{z}}e^{-jk_0 z}\right\} \tag{3-51}$$

And C_m for m<0 is given by

$$C_m \approx u_0\left\{e^{-j\frac{\pi}{4}}\sqrt{\lambda}D(\theta_m,\theta_{in})e^{-j\frac{m\pi}{2}}e^{-jk_m z}-(-1)^m\frac{4dD(0,\theta_{in})}{jm\pi\sqrt{z}}e^{-jk_0 z}\right\} \tag{3-52}$$

As before, for $z >> d^2/\lambda$ we may neglect the second term in (3-51) and (3-52).

From the result of (3-51) and (3-52), the diffracted modal electric field due to the diffraction at the right hand edge in the tunnel is expressed as

$$E_y(x,z) = -u_0 e^{j\frac{\pi}{4}} \frac{\sqrt{\lambda}}{2d} \left\{ \sum_{m=odd} (-1)^{\frac{m-1}{2}} D(\theta_m, \theta_{in}) \cos\left(\frac{m\pi}{2d}x\right) e^{-jK_m z} \right.$$
$$\left. - \sum_{m=even} (-1)^{\frac{m}{2}} D(\theta_m, \theta_{in}) \sin\left(\frac{m\pi}{2d}x\right) e^{-jK_m z} \right\} \qquad (3\text{-}53)$$

3.3 Mode Diffraction in 2-D Cross Tunnels

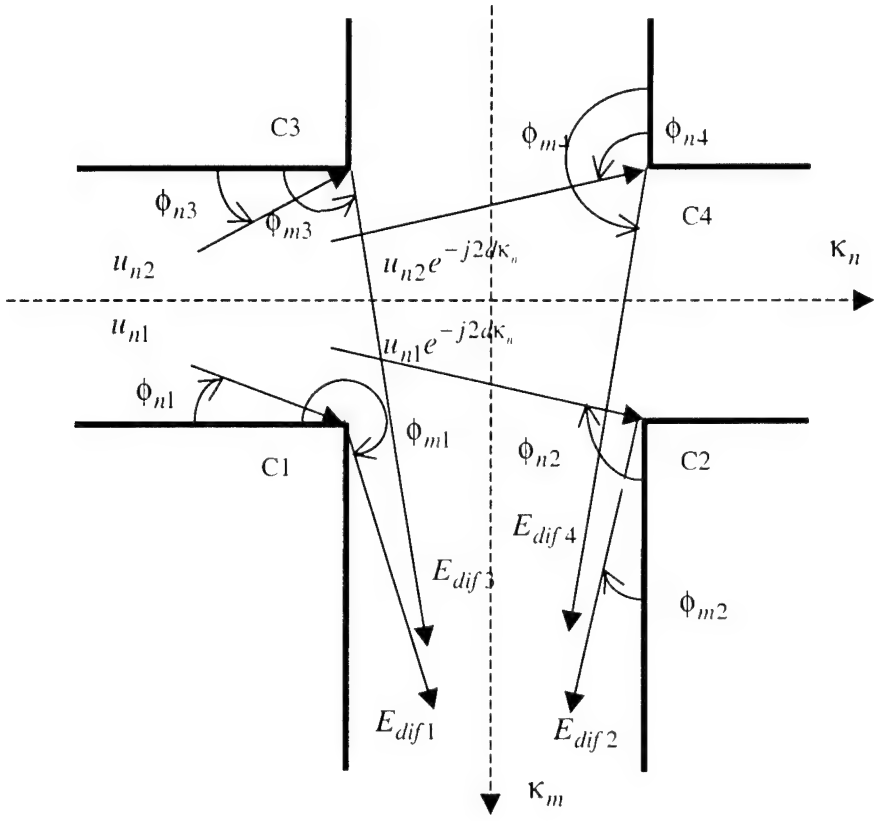

Figure 3-7 Mode Diffraction in 2-D Cross-Tunnels

For a 2-D cross tunnels we suppose that the n^{th} mode is incident from the left in the primary waveguide. The modal fields excited in the cross arms are then generated by diffraction at the four corner edges (C1,C2,C3 and C4), as indicated in Figure 3-7 for the fields in the lower arm. Let $E_y(x.z)_{C1,C2} = E_{dif1} + E_{dif2}$ be the field in the lower cross arm due to diffraction at the left hand corners C1 and C2. These contribution to the total field were derived in the previous section. Assuming both the main tunnel and cross arm to have width 2d, this contribution to the field is given by the modal sum

$$E_y(x,z)_{C1,C2} =$$

$$u_{n1}e^{j\frac{\pi}{4}}\frac{\sqrt{\lambda}}{2d}\left\{\sum_{m=odd}(-1)^{\frac{m-1}{2}}D(\phi_{m1},\phi_{n1})\cos(\beta_m x)e^{-j\kappa_m z}-\sum_{m=even}(-1)^{\frac{m}{2}}D(\phi_{m1},\phi_{n1})\sin(\beta_m x)e^{-j\kappa_m z}\right\}$$

$$+u_{n1}e^{-j2d\kappa_n}e^{j\frac{\pi}{4}}\frac{\sqrt{\lambda}}{2d}\left\{\sum_{m=odd}(-1)^{\frac{m-1}{2}}D(\phi_{m2},\phi_{n2})\cos(\beta_m x)e^{-j\kappa_m z}-\sum_{m=even}(-1)^{\frac{m}{2}}D(\phi_{m2},\phi_{n2})\sin(\beta_m x)e^{-j\kappa_m z}\right\} \quad (3\text{-}54)$$

Here u_{n1} is the amplitude of the field incident on corner C1, while the field incident on the corner C2 differs by the phase factor $e^{-j2d\kappa_n}$.

In addition to the diffraction at the right hand corners, diffraction at the upper corners generate $E_y(x.z)_{C3,C4} = E_{dif3} + E_{dif4}$, which is given by

$$E_y(x,z)_{C3,C4} =$$

$$-u_{n2}e^{j\frac{\pi}{4}}\frac{\sqrt{\lambda}}{2d}\left(\sum_{m=odd}(-1)^{\frac{m-1}{2}}D(\phi_{m4},\phi_{n4})\cos(\beta_m x)e^{-j\kappa_m(z+2d)}\right.$$

$$\left.-\sum_{m=even}(-1)^{\frac{m}{2}}D(\phi_{m4},\phi_{n4})\sin(\beta_m x)e^{-j\kappa_m(z+2d)}\right\} \quad (3\text{-}55)$$

$$-u_{n2}e^{-j2d\kappa_n}e^{j\frac{\pi}{4}}\frac{\sqrt{\lambda}}{2d}\left\{\sum_{m=odd}(-1)^{\frac{m-1}{2}}D(\phi_{m3},\phi_{n3})\cos(\beta_m x)e^{-j\kappa_m(z+2d)}\right.$$

$$\left.-\sum_{m=even}(-1)^{\frac{m}{2}}D(\phi_{m3},\phi_{n3})\sin(\beta_m x)e^{-j\kappa_m(z+2d)}\right\}$$

The term u_{n2} is the amplitude of the field incident on corner C3, while the field incident on the corner C4 is $u_{n2}e^{-j2d\kappa_n}$. The various diffraction angle in (3-54), (3-55) are as shown in Figure 3-7. Also, the fields u_{n1} and u_{n2} represent $E_y{}^n$ of the n^{th} mode at the lower and upper walls of the main tunnel. For line source excitation, they are given by

$$E_y{}^n(x=\pm d, z=L) = \frac{-\omega\mu_0}{2d} J_0 \begin{cases} \left[\sin(\beta_n(\pm d))\sin(\beta_n x')\frac{e^{-j\kappa_n L}}{\kappa_n}\right]_{n=even} \\ \left[\cos(\beta_n(\pm d))\cos(\beta_n x')\frac{e^{-j\kappa_n L}}{\kappa_n}\right]_{n=odd} \end{cases} \quad (3\text{-}56)$$

where L is the distance from the transmitter to the corner. The total modal field in the cross arm is then given by a summation over the incident modes in the main tunnel, or

$$E_y{}^{dif}(x,z) = \sum_{n=1}^{\infty}\left(E_y(x,z)_{C1,C2} + E_y(x,z)_{C3,C4}\right) \quad (3\text{-}57)$$

To find the field in 2-D cross tunnels due to point source in the main tunnel requires the inclusion of the field spreading of the plane of the cross section. For the lower modes having κ_n close to k_0, the spreading is account for by multiplying (3-56) by the factor $e^{j\frac{\pi}{4}}\frac{\sqrt{k_0}}{\sqrt{2\pi(z+L)}}$. In order to study the effect of the diffraction into the cross arm on the received signal, we have compared the received power as a function of distance along a straight tunnel to the received power as a function of distance along a cross arm located L = 500 m from the source. Because of the various phase terms in the sums, the fields show considerable local variation over a wavelength scale. Some of this variation can be removed by averaging the received power over the cross section of the tunnel. Figure 3-8 shows the average received power as a function of distance for vertically polarized antennas operating at 900 MHz. Both tunnels are 4 m wide and the walls have dielectric constant $\varepsilon_r = 6$ and conductance $\sigma = 0.01$. The 1 watt transmitter is located in middle of the tunnel (2 m from the tunnel wall). The UTD diffraction coefficients proposed by Luebbers [12] have been used for the calculation. We found that the coupling loss of cross-junction tunnel is about 37 dB for this case. Plots of power received in the cross tunnel for 300MHz and 100 MHz sources are shown in Figure 3-9

and 3-10. For these computations, the corners are located at L=50 m from the transmitter and coupling loss is found to be 28 and 23 dB, respectively.

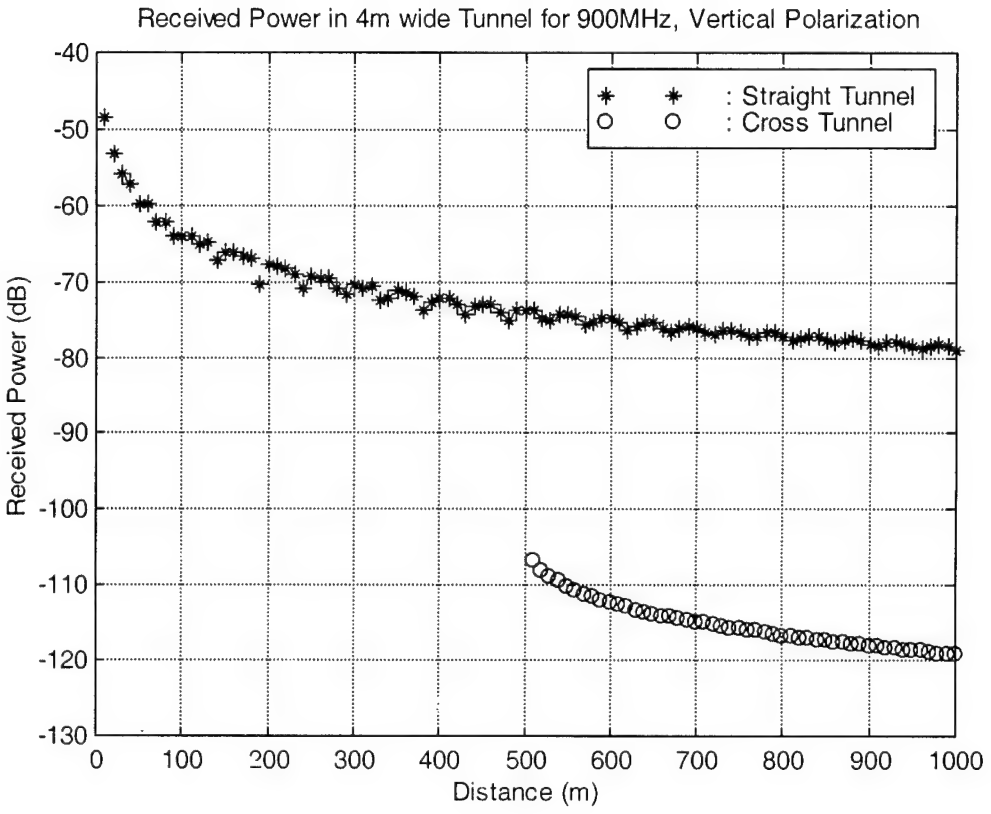

Figure 3-8 Received Power in 4 m wide 2-D Straight and Cross-junction Tunnels

900 MHz, Vertical Polarization, $\varepsilon_r = 6, \sigma = 0.01$

The corner of cross-junction Tunnel is located at 500 m.

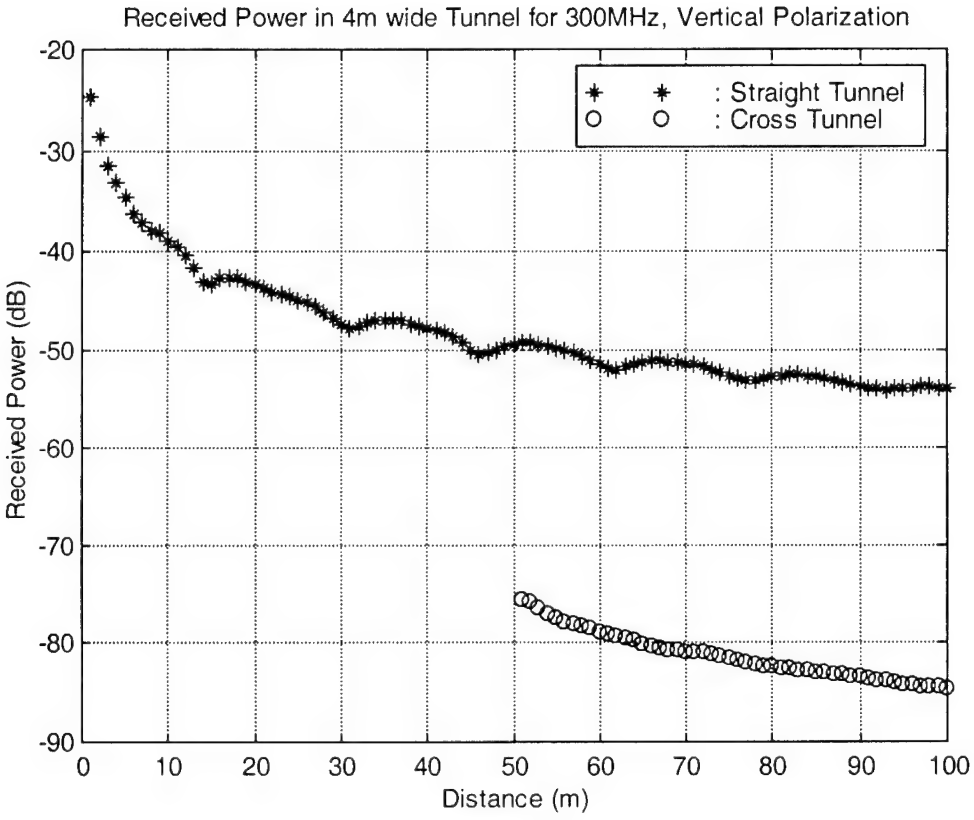

Figure 3-9 Received Power in 4 m wide 2-D Straight and Cross-junction Tunnels

300MHz, Vertical Polarization, $\varepsilon_r = 6, \sigma = 0.01$

The corner of cross-junction Tunnel is located at 50 m.

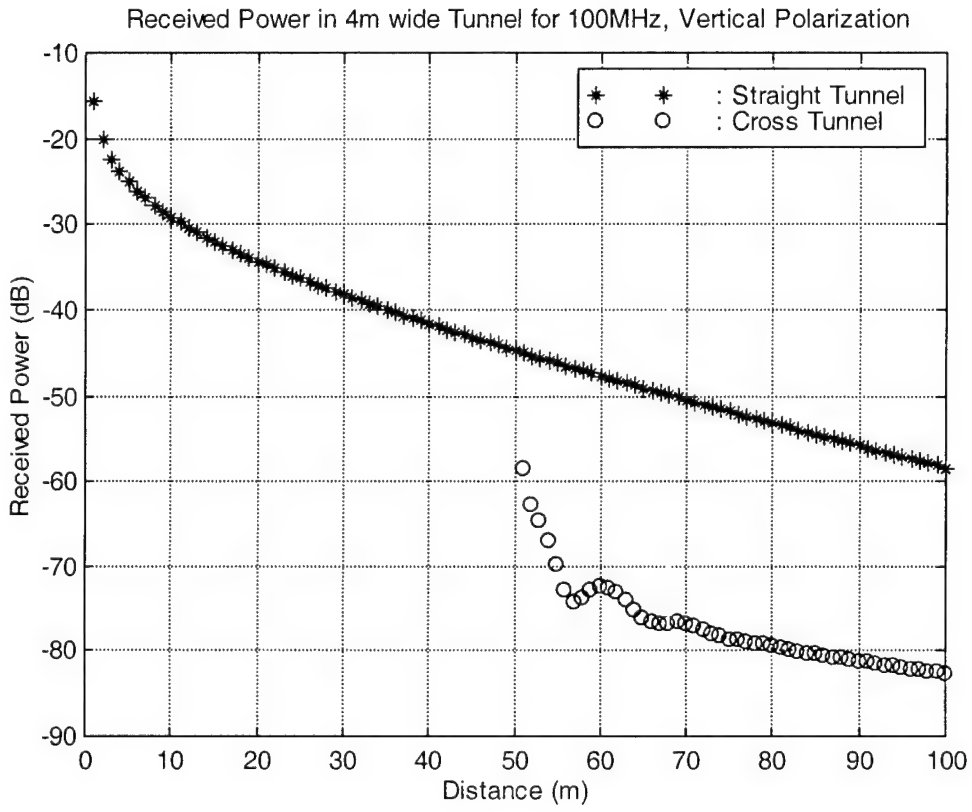

Figure 3-10 Received Power in 4 m wide 2-D Straight and Cross-junction Tunnels

100 MHz, Vertical Polarization, $\varepsilon_w = 6, \sigma = 0.01$

The corner of cross-junction Tunnel is located at 50 m.

3.4 Mode Diffraction in 2-D T-Tunnels

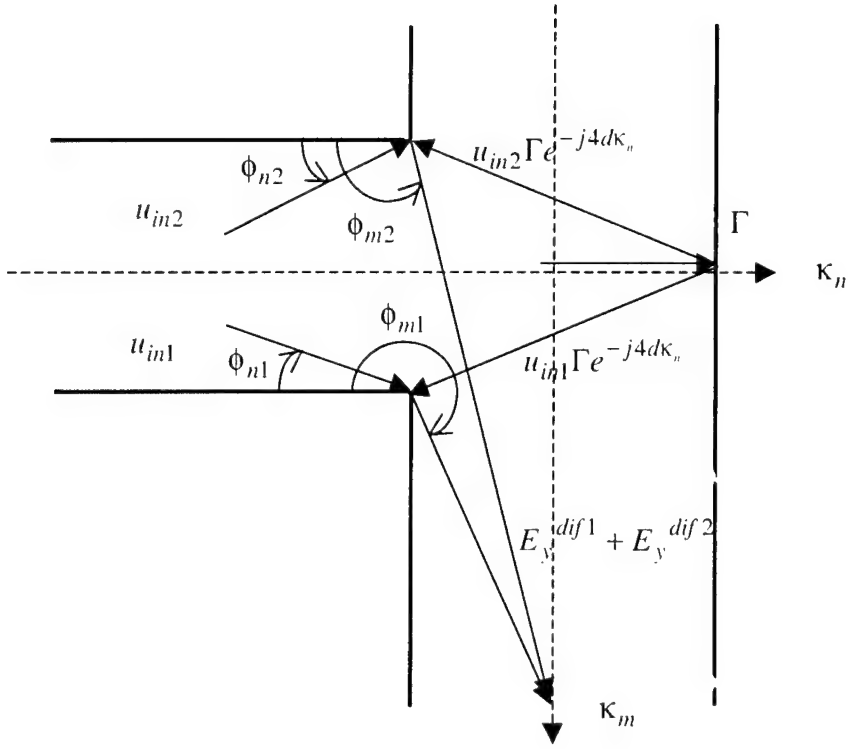

Figure 3-11 Mode Diffraction in 2-D T-junction Tunnels

When a modal field is incident on a T junction, as shown in Figure 3-11 it illuminates the two corners directly, and indirectly via reflection at the further wall. For $d >> \lambda$ the reflected field will be essentially the same as that of two incident mode, except for a reflection coefficient Γ. Because the mode angle ϕ_n are small, Γ will be close to the value for a plane wave at normal incidence. Let $E_y^{dif1}(x,z)$ represent the modal field in the lower arm of the junction due to the n^{th} mode incident directly from the horizontal tunnel in Figure 3-11 into the upper and lower corners. This sum is given by

$$
\begin{aligned}
&E_y^{dif1}(x,z) = \\
&u_{n1} e^{j\frac{\pi}{4}} \frac{\sqrt{\lambda}}{2d} \left\{ \sum_{m=odd} (-1)^{\frac{m-1}{2}} D(\phi_{m1},\phi_{n1}) \cos(\beta_m x) e^{-j\kappa_m z} \right. \\
&\left. - \sum_{m=even} (-1)^{\frac{m}{2}} D(\phi_{m1},\phi_{n1}) \sin(\beta_m x) e^{-j\kappa_m z} \right\} \\
&- u_{n2} e^{j\frac{\pi}{4}} \frac{\sqrt{\lambda}}{2d} \left\{ \sum_{m=odd} (-1)^{\frac{m-1}{2}} D(\phi_{m2},\phi_{n2}) \cos(\beta_m x) e^{-j\kappa_m (z+2d)} \right. \\
&\left. - \sum_{m=even} (-1)^{\frac{m}{2}} D(\phi_{m2},\phi_{n2}) \sin(\beta_m x) e^{-j\kappa_m (z+2d)} \right\}
\end{aligned}
\tag{3-58}
$$

Similarly, let $E_y^{dif2}(x,z)$ represent the modal field resulting from diffraction at the corners resulting from the incident mode field that is reflected from the wall. This sum is given by

$$
\begin{aligned}
&E_y^{dif2}(x,z) = \\
&u_{n1} \Gamma e^{-j4d\kappa_n} e^{j\frac{\pi}{4}} \frac{\sqrt{\lambda}}{2d} \left\{ \sum_{m=odd} (-1)^{\frac{m-1}{2}} D\left(\phi_{m1}{}^r,\phi_{n1}{}^r\right) \cos(\beta_m x) e^{-j\kappa_m z} \right. \\
&\left. - \sum_{m=even} (-1)^{\frac{m}{2}} D\left(\phi_{m1}{}^r,\phi_{n1}{}^r\right) \sin(\beta_m x) e^{-j\kappa_m z} \right\} \\
&- u_{n2} \Gamma e^{-j4d\kappa_n} e^{j\frac{\pi}{4}} \frac{\sqrt{\lambda}}{2d} \left\{ \sum_{m=odd} (-1)^{\frac{m-1}{2}} D\left(\phi_{m2}{}^r,\phi_{n2}{}^r\right) \cos(\beta_m x) e^{-j\kappa_m (z+2d)} \right. \\
&\left. - \sum_{m=even} (-1)^{\frac{m}{2}} D\left(\phi_{m2}{}^r,\phi_{n2}{}^r\right) \sin(\beta_m x) e^{-j\kappa_m (z+2d)} \right\}
\end{aligned}
\tag{3-59}
$$

In (3-59), Γ is taken to be the plane wave reflection coefficient for normal incidence. The incident fields u_{n1} and u_{n2} are given by (3-56).

The total field in the lower arm is then given by

$$
E_y^{dif}(x,z) = \sum_{n=1}^{\infty} \left[E_y^{dif1}(x,z) + E_y^{dif2}(x,z) \right] \tag{3-60}
$$

Computation have been made for the received power averaged over the cross section in the main tunnel and in the side tunnels for a T junction. The tunnels are 4 m wide and the walls have dielectric constant $\varepsilon_r = 6$ and conductance $\sigma = 0.01$. Figure 3-12 shows received power in straight tunnel, and in the arm of a T junction for a vertically polarized, 900MHz transmitter located in the middle of the main tunnel (2m from the each wall) and 500m from the T junction. The coupling loss into the T junction tunnel is about 42 dB for this case. The received power for 300 MHz and 100 MHz sources are shown in Figure 3-13 and 3-14 when the sources are located at 50m from T junction. The coupling loss for theses two frequencies is about 31 and 29 dB, respectively.

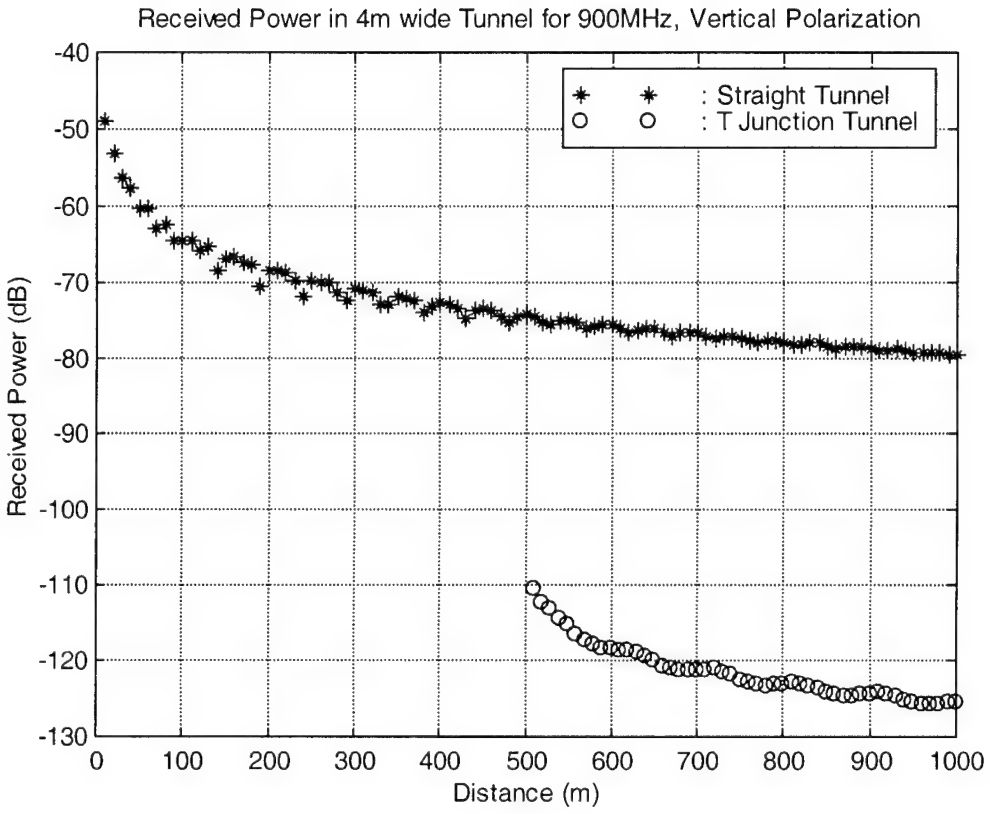

Figure 3-12 Received Power in 4 m wide 2-D Straight and T-Junction Tunnels

900MHz, Vertical Polarization , $\varepsilon_w = 6, \sigma = 0.01$

The corner of T-Junction Tunnel is located at 500 m.

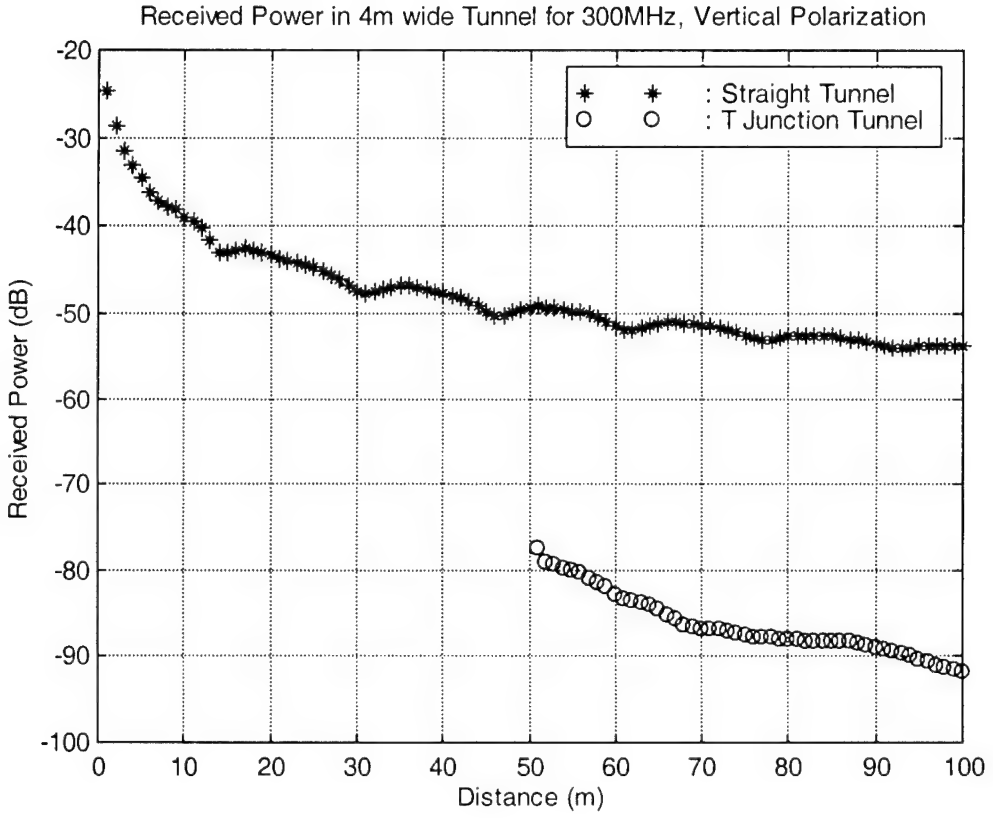

Figure 3-13 Received Power in 4 m wide 2-D Straight and T-Junction Tunnels

300MHz, Vertical Polarization , $\varepsilon_w = 6, \sigma = 0.01$

The corner of T-Junction Tunnel is located at 50 m.

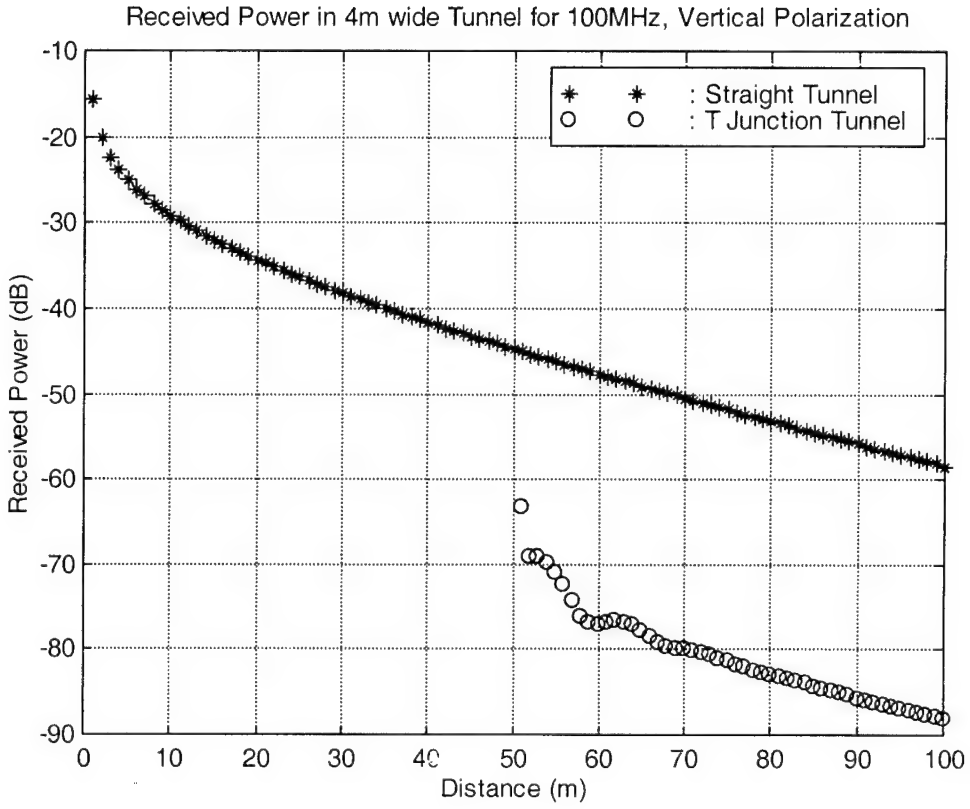

Figure 3-14 Received Power in 4 m wide 2-D Straight and T-Junction Tunnels

100MHz, Vertical Polarization , $\varepsilon_w = 6, \sigma = 0.01$

The corner of T-Junction Tunnel is located at 50 m.

3.5 Mode Propagation in 2-D L-Tunnels

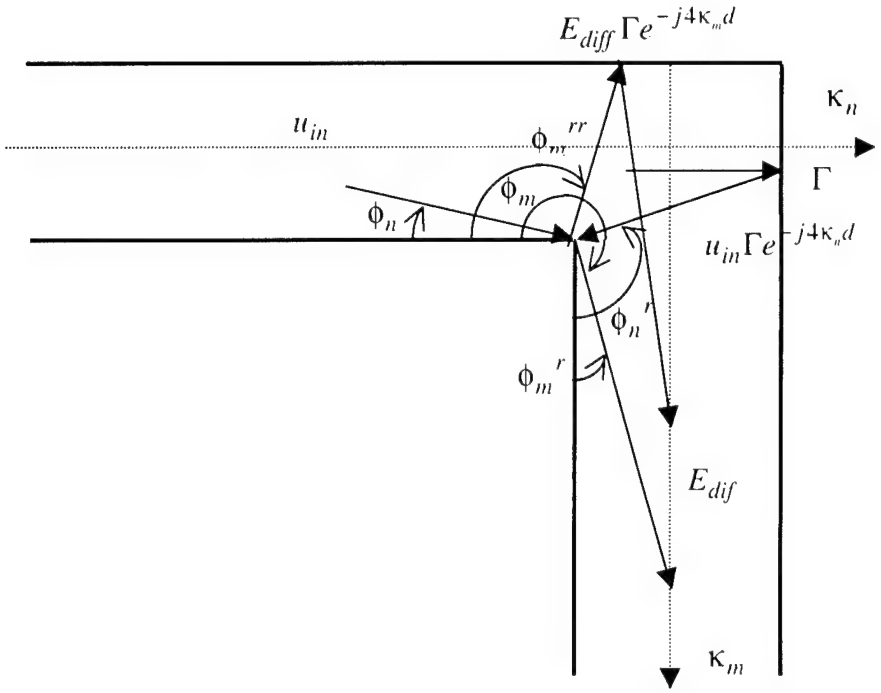

Figure 3-15 Mode Diffraction in L-bend Tunnels

When turning the corner in an L shaped tunnel, the diffraction takes place at the single corner shown in Figure 3-15. However, reflection in the opposite wall produces additional contributions to the modal fields. One contribution to the modal field in the arm of the tunnel is directly diffracted field $E_y{}^{dif1}(x,z)$ that is diffracted through the angle ϕ_m, and caused by the field incident at the mode angle ϕ_n. A second field $E_y{}^{dif2}(x,z)$ results from the reflection of the incident mode at the wall, seen on the right in Figure 3-15. The incident angle for this field is $\phi_n{}^r = \phi_n + \pi/2$, while the angle of the diffracted ray is $\phi_m{}^r$ in Figure 3-12. The third field $E_y{}^{dif3}(x,z)$ from the reflection of a

diffracted ray at the top wall in Figure 3-15. In this case the diffraction angle is $\phi_m{}^{rr}$. This third contribution is generated by both the incident modal field, and by the modal field reflected in the right hand wall in Figure 3-15. However, because of the reduction in strength due to the reflection coefficient for near normal incidence, we include only the contribution from the incident normal field. The modal field in the tunnel arm is

$$E_y{}^{dif}(x,z) = \sum_{n=1}^{\infty}\left[E_y{}^{dif\,1}(x,z) + E_y{}^{dif\,2}(x,z) + E_y{}^{dif\,3}(x,z)\right] \tag{3-61}$$

The modal diffracted field from the single corner $E_y{}^{dif\,1}(x,z)$ is expressed as

$$E_y{}^{dif\,1}(x,z) = u_n e^{j\frac{\pi}{4}} \frac{\sqrt{\lambda}}{2d}\left\{\sum_{m=odd}(-1)^{\frac{m-1}{2}} D(\phi_m,\phi_n)\cos(\beta_m x)e^{-j\kappa_m z} - \sum_{m=even}(-1)^{\frac{m}{2}} D(\phi_m,\phi_n)\sin(\beta_m x)e^{-j\kappa_m z}\right\} \tag{3-62}$$

where the incident modal fields u_n at the corner is given by (3-56).

The fields $E_y{}^{dif\,2}(x,z)$, $E_y{}^{dif\,3}(x,z)$ are of the same form as to (3-62), but are multiplied by the normal reflection coefficient $\Gamma = \dfrac{1-\sqrt{\varepsilon_w}}{1+\sqrt{\varepsilon_w}}$ for the wall with dielectric constant ε_w, have a different diffraction coefficient, and phase factor due to the additional propagation distance in the vicinity of the corner. Thus

$$E_y{}^{dif\,2}(x,z) = u_n \Gamma e^{-j4\kappa_n d} e^{j\frac{\pi}{4}} \frac{\sqrt{\lambda}}{2d}\left\{\sum_{m=odd}(-1)^{\frac{m-1}{2}} D\left(\phi_m{}^r,\phi_n{}^r\right)\cos(\beta_m x)e^{-j\kappa_m z}\right. \tag{3-63}$$
$$\left. - \sum_{m=even}(-1)^{\frac{m}{2}} D\left(\phi_m{}^r,\phi_n{}^r\right)\sin(\beta_m x)e^{-j\kappa_m z}\right\}$$

and

$$
\begin{aligned}
&E_y^{dif3}(x,z) = \\
&u_n \Gamma e^{-j4\kappa_m d} e^{j\frac{\pi}{4}} \frac{\sqrt{\lambda}}{2d} \left\{ \sum_{m=odd} (-1)^{\frac{m-1}{2}} D\left(\phi_m{}^{rr}, \phi_n\right) \cos(\beta_m x) e^{-j\kappa_m z} \right. \\
&\left. - \sum_{m=even} (-1)^{\frac{m}{2}} D\left(\phi_m{}^{rr}, \phi_n\right) \sin(\beta_m x) e^{-j\kappa_m z} \right\}
\end{aligned}
\tag{3-64}
$$

The received powers in an averaged over the cross section for vertically polarized sources in a straight tunnel and in an L-Bend tunnel are shown in Figure 3-16 ~ 18. The width of both tunnels is 4 m and the walls have the dielectric constant $\varepsilon_r = 6$ and conductance $\sigma = 0.01$. Figure 3-16 shows the results for a 900MHz source located 500 m from the L bend, and centered in tunnel. The UTD diffraction coefficients [12] are used for this simulation. The coupling loss of the 4 m wide L-Bend tunnel is about 50 dB for this case. Figure 3-17 and 3-18 show the received power for 300 MHz and 100 MHz sources located at 50 m from L bend. The turning loss for these two frequencies is about 35 dB, and 30 dB respectively.

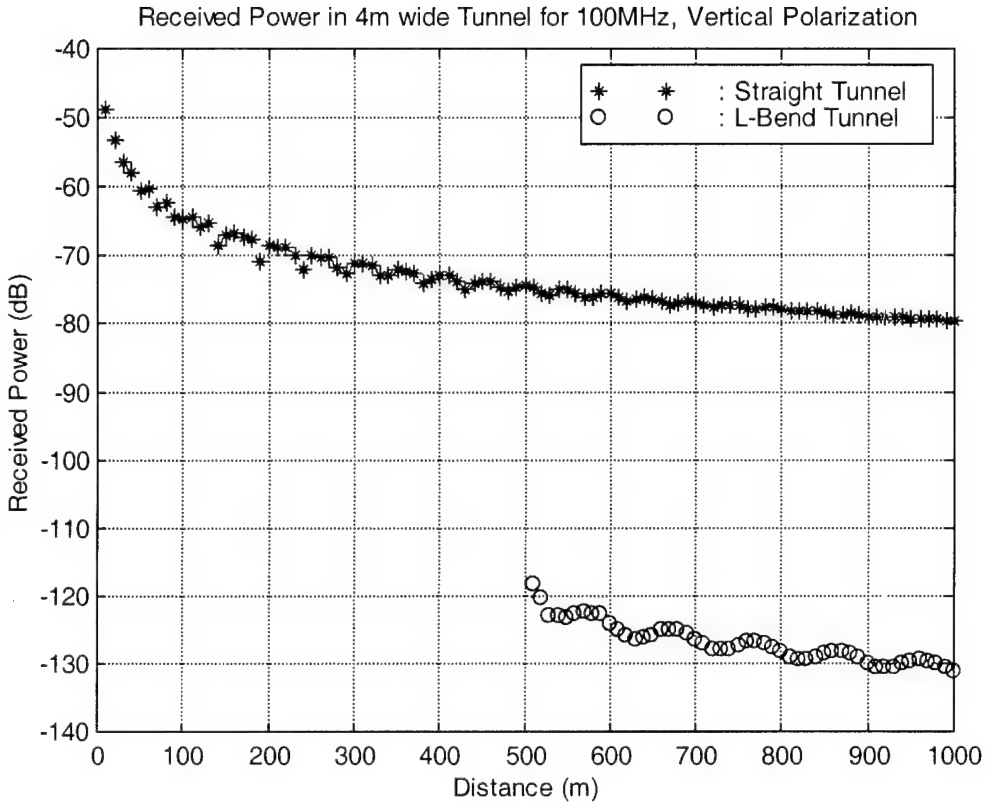

Figure 3-16 Received Power in 4 m wide 2-D Straight and L bend Tunnel

900 MHz, Vertical Polarization , $\varepsilon_r = 6, \sigma = 0.01$

The corner of L-Bend Tunnel is located at 500 m.

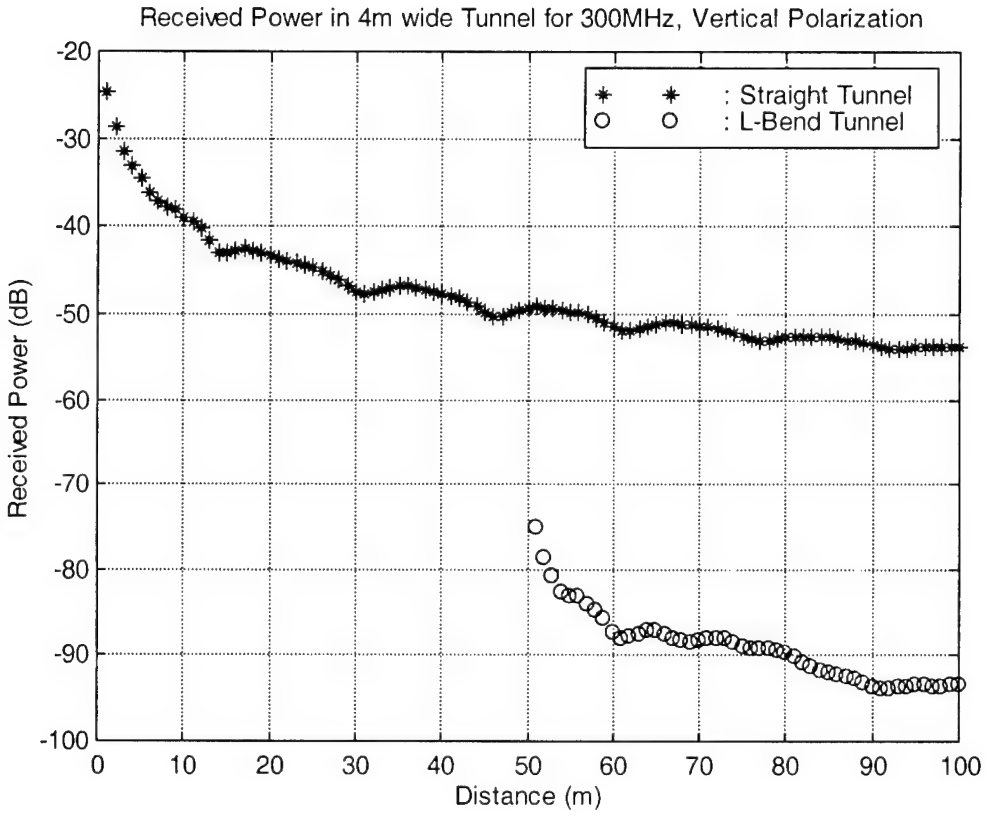

Figure 3-17 Received Power in 4 m wide 2-D Straight and L bend Tunnel

300 MHz, Vertical Polarization , $\varepsilon_r = 6, \sigma = 0.01$

The corner of L-Bend Tunnel is located at 50 m.

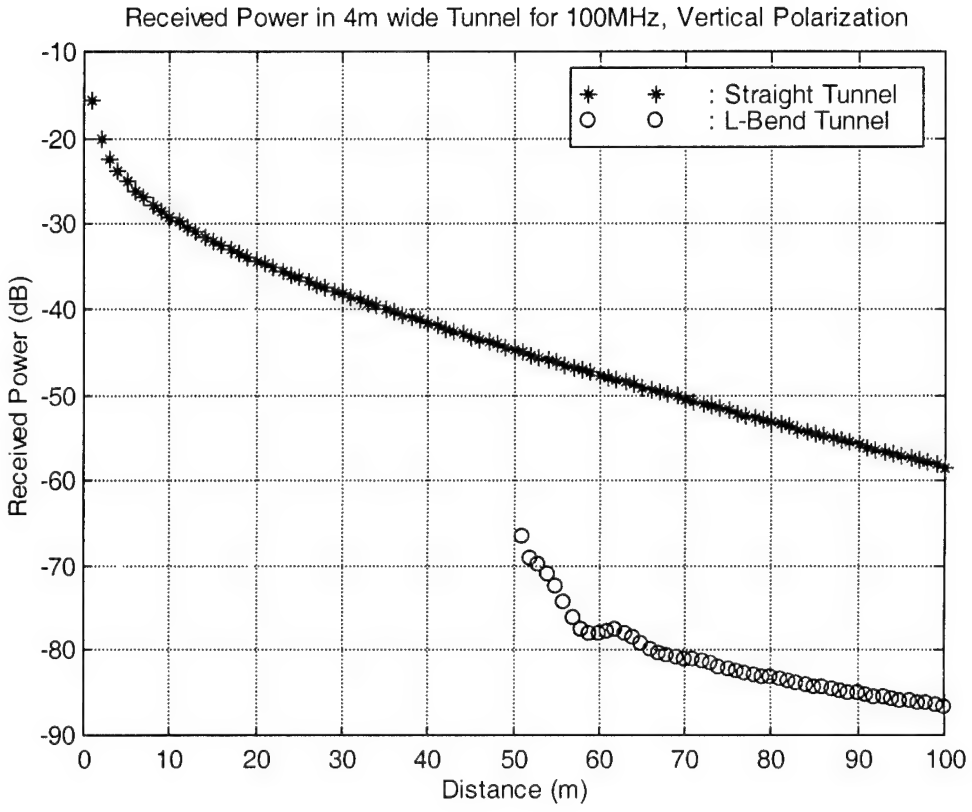

Figure 3-18 Received Power in 4 m wide 2-D Straight and L bend Tunnel

100 MHz, Vertical Polarization , $\varepsilon_r = 6, \sigma = 0.01$

The corner of L-Bend Tunnel is located at 50 m.

4. Propagation in Rectangular 3-D Tunnels

4.1 Fields in a Rectangular 3-D Tunnel for Point Source Excitation

The modal fields in straight 3-D tunnels of rectangular cross section are approximately the product of the modal variations for 2-D tunnels [2]. For the vertical polarization of the electric field in a 3-D tunnel, the power loss of side walls is due to TE attenuation and the power loss of ceiling and floor is due to TM attenuation. Because the spatial dependence in both transverse x and y direction can be either a cosine or a sine variation, the modal field in 3-D tunnel have four possible combination of x and y dependence. These combinations are : 1) sine variation in both x and y; 2) sine variation in x and cosine in y; 3) cosine variation in x and sine in y; 4) cosine variation both in x and y. To simplify the field expressions, we place the transmitter at center of the tunnel $(x' = 0, y' = 0)$, so that only the symmetric modes are excited. For vertical polarization of the electric field, the symmetric modes have dependence

$$E_y = \sum_{m=odd} \sum_{n=odd} A_{m,n} \cos\left(\beta_m{}^{TE} x\right) \cos\left(\beta_n{}^{TM} y\right) e^{-j\kappa_{m,n} z} \tag{4-1}$$

For a tunnel of width $2d_1$ and height $2d_2$

$$\beta_m{}^{TE} = \frac{m\pi}{2d_1} + j\frac{m\lambda}{4d_1{}^2\sqrt{\varepsilon_w - 1}} \tag{4-2}$$

$$\beta_n{}^{TM} = \frac{n\pi}{2d_2} + j\frac{n\varepsilon_w\lambda}{4d_2{}^2\sqrt{\varepsilon_w - 1}} \tag{4-3}$$

$$\kappa_{m,n} = \sqrt{k_0{}^2 - \beta_m^{TE\,2} - \beta_n^{TM\,2}} \approx \sqrt{k_0{}^2 - \left(\frac{m\pi}{2d_1}\right)^2 - \left(\frac{n\pi}{2d_2}\right)^2} - j\left(\frac{m^2\lambda^2}{16d_1{}^3\sqrt{\varepsilon_w - 1}} + \frac{n^2\varepsilon_w\lambda^2}{16d_2{}^3\sqrt{\varepsilon_w - 1}}\right) \tag{4-4}$$

The attenuation constant of the modes is dominated by the term $n^2\varepsilon_w$, which causes the attenuation to be like that of a TM polarization in a 2-D tunnel.

The spatial dependence of the current distribution for a point source located at $y = 0$ can be expressed in terms of the Fourier sum

$$I_o h\delta(y) = I_0 h + \frac{I_0 h}{d_2} \sum_{n=even} \cos\left(\frac{n\pi}{2d_2} y\right) \tag{4-5}$$

The cosine terms in (4-1) can be thought of as resulting from two line sources with phase variation $e^{\pm j\frac{n\pi}{2d}y}$. The phased line sources in a 2-D tunnel produces total field having y dependence $\cos\left(\frac{n\pi}{2d} y\right)$ which is close to that of the modal field in (2-53). As a result, the modal field for vertical polarization in a 3-D tunnel is given by

$$E_y(x, y, z) \approx \left(\frac{-I_0 h}{4d_1 d_2}\right)\left\{\sum_{m=odd}\sum_{n=odd}\left(\frac{\omega\mu_0}{\kappa_{m,n}}\right)\cos\left(\beta_m{}^{TE} x\right)\cos\left(\beta_n{}^{TM} y\right)e^{-j\kappa_{m,n}z}\right\} \tag{4-6}$$

Figure 4-1 shows the received power in 3-D tunnel (4m wide, 3m high) for vertically polarized 900MHz signal. The received power is averaged over the section at 1.5 m high from the floor and the transmitter is centered and at the mouth of tunnel. The reference position for normalization is at 10 m from the source and it is -55dB at reference point. The free space received power at this point is –51.5 dB. The normalized path gain for an isotropic point source in a 3-D straight tunnel is shown Figure 4-2. For this calculation, the dimension of tunnel is assumed to be $2d_1 = 4$ m and $2d_2 = 3$ m. The transmitter is oriented vertically at the center of the tunnel width and height. In order to define the normalized path gain, $|E_y|^2$ is averaged over the width of tunnel at 1.5 m high from floor. This value is then normalized to the value of the average at z = 10 m. Because the tunnel height is smaller than its width, and because the attenuation due to reflection of TM polarized waves at the ceiling and floor dominates over that due to TE reflection at the walls, the attenuation in the tunnel is greater than either the TE or TM case in a 2-D

tunnel of width 4 m. As in the case of a 2-D tunnel, lower frequency signals undergo much higher attenuation.

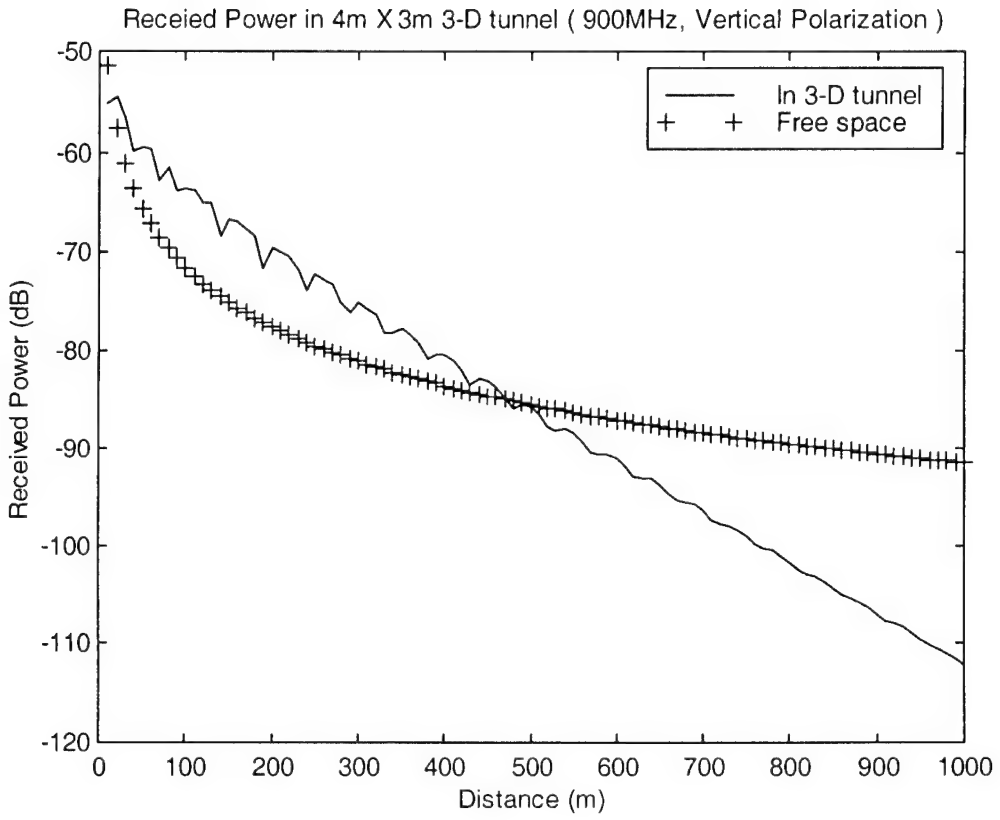

Figure 4-1 Received Power in 3-D straight tunnel (4m wide, 3m high) for 900MHz, Vertical Polarization (ε_w=6, σ = 0.01)

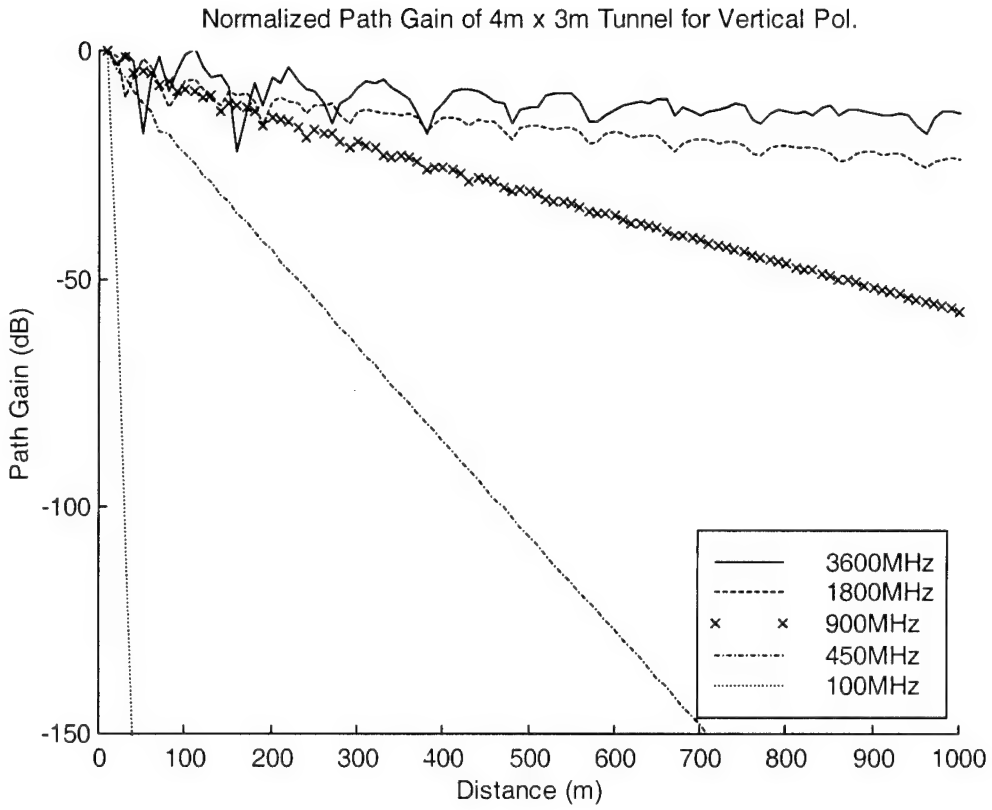

Figure 4-2 Normalized Path Gain in 3-D straight tunnel (4m wide, 3m high)

for various frequencies

Vertical Polarization (ε_w =6, $\sigma = 0.01$)

4.2 Attenuation of modal field in 3-D tunnels

The attenuation constant in a 3-D tunnel that is $2d_1$ m wide and $2d_2$ m high is defined by (4-7) for vertical polarization and (4-8) for horizontal polarization from (4-6).

$$\alpha(dB) = 20\log\left(e^{\mathrm{Im}(\kappa_{m,n})}\right) \approx \frac{10}{\ln 10}\left[\frac{m^2\lambda^2}{(2d_1)^3\sqrt{\varepsilon_w - 1}} + \frac{n^2\varepsilon_w\lambda^2}{(2d_2)^3\sqrt{\varepsilon_w - 1}}\right] \tag{4-7}$$

$$\alpha(dB) = 20\log\left(e^{\mathrm{Im}(\kappa_{m,n})}\right) \approx \frac{10}{\ln 10}\left[\frac{m^2\varepsilon_w\lambda^2}{(2d_1)^3\sqrt{\varepsilon_w - 1}} + \frac{n^2\lambda^2}{(2d_2)^3\sqrt{\varepsilon_w - 1}}\right] \tag{4-8}$$

where ε_w is dielectric constant of tunnel walls. In Figure 4-3, we showed the attenuation constant per 100 m for dominant mode (m=1,n=1) vs the ratio of tunnel width and height in 3-D tunnels. The tunnel height is assumed to be $2d_2$ =4 m high and the operating frequency is 900 MHz for this plot. The dielectric constant of tunnel walls and both ceiling and floor is used ε_w=6. If the width of tunnel is greater than the height, then the attenuation of horizontal polarization is lower than vertical polarization. Otherwise, the vertical polarization gives lower attenuation in 3-D tunnel. By (4-7) and (4-8), the polarization for low attenuation is determined by comparing the two dimension terms with dielectric constant.

The attenuation of dominant mode (1,1) versus $\frac{\lambda^2}{d^3}$ for 3-D tunnels having square cross section is shown in Figure 4-4. As we discussed in connection with the attenuation in 2-D tunnels, the attenuation increases rapidly when the wavelength of given frequency is close to the tunnel dimension. Higher modes attenuate even more rapidly. In order to quantify this, let $\Delta L = \frac{10}{\alpha_{11}} - \frac{10}{\alpha_{21}}$ be the distance at which the next higher mode (2,1) attenuates by 10 dB more than the dominant (1,1) mode. The variation of ΔL with the parameter $\frac{\lambda^2}{d^3}$ in a 3-D tunnel with square cross section is illustrated in Figure 4-5. For

example, in a 4m×4m tunnel and at a frequency of 900MHz, $\frac{\lambda^2}{d^3} \approx 1.42\times10^{-2}$. From Figure 4-4 it is seen that in just over 100m the (2,1) mode is reduced by 10dB as compared to the (1,1) mode. At 300MHz, this distance is only about 15m.

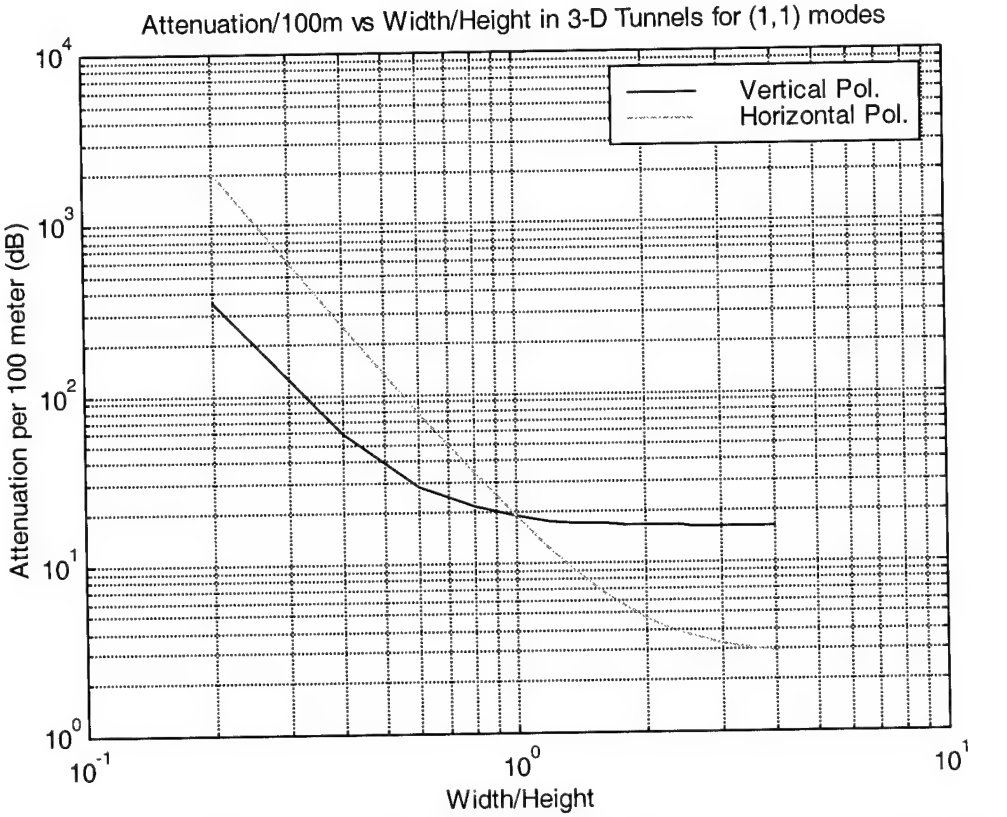

Figure 4-3 Attenuation constant for dominant mode vs the ratio of the width and height in 3-D tunnels for $\varepsilon_r = 6$ (900MHz, 4m tunnel height)

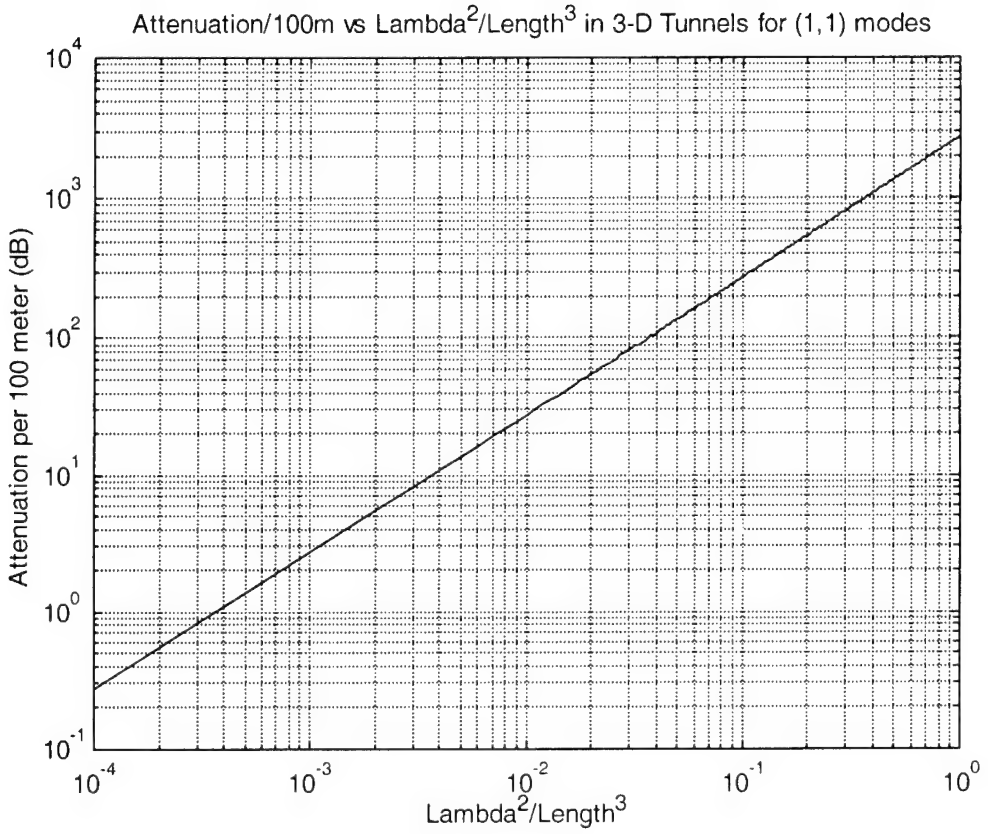

Figure 4-4 Attenuation constant vs $\frac{\lambda^2}{d^3}$ for dominant mode in 3-D square tunnels

(Dielectric constant $\varepsilon_w = 6$)

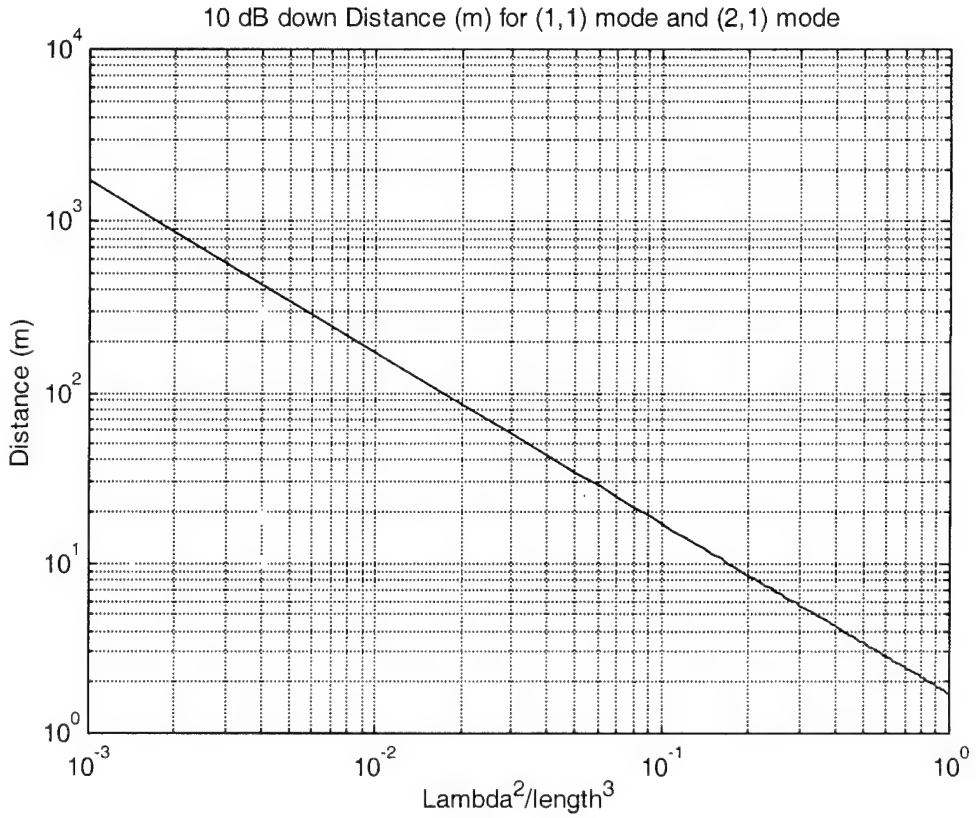

Figure 4-5 Distance for 10 dB down of (1,1) and (2,1) mode vs $\frac{\lambda^2}{d^3}$

in 3-D square tunnels (Dielectric constant $\varepsilon_w = 6$)

4.3 Coupling loss at L, T, Cross junctions

The coupling loss at junctions in 3-D tunnels will occur via diffraction at the corners, as previously discussed for 2-D tunnels. If the height of the main tunnel and side tunnel are the same, then the modes excited in the cross tunnel will have the same field variation in the vertical direction as the incident mode. For the lower modes the diffraction coefficient at the edge will be nearly the same as in the 2-D tunnel were there is no variation along the edge. Since the coupling is nearly independent of the mode number in the vertical direction, the coupling loss for 3-D tunnels is the same as for 2-D tunnels, and is independent of tunnel height.

The coupling loss vs various tunnel width for L-bend, T junction and cross junction structure for 900MHz vertical polarization is shown in Figure 4-6. The coupling loss of cross tunnels is about 3 dB lower than T-junction tunnels. The diffracted fields in cross tunnels have no wall reflection factor for comparing with the T-junction so that the coupling loss of T-junction tunnels is higher than cross tunnels. (See Figure 3-7 and 3-11) The coupling loss of L-bend tunnels is about 8 dB higher than T-junction tunnels. We find the diffracted fields in T-junction have one more upper edge diffraction fields by comparing with Figure 3-8 and 3-10. The incident angle for upper edge is smaller than lower edge for given same diffracted angle so that the diffraction coefficient of upper edge is larger than lower edge. Therefore the coupling loss of T-junction is smaller than the L-bend tunnels.

If we take into account only the (1,1) mode in the main and side tunnels, then the received powers in the cross, T and L junctions at y=0 are respectively

$$E_y(x, y=0, z)_{cross} =$$
$$u_{in} e^{j\frac{\pi}{4}} \frac{\sqrt{\lambda}}{4 d_1 d_2} \left(D_{C1} + D_{C2} e^{-j2d_1\kappa_{11}} - \left(D_{C3} + D_{C4} e^{-j2d_1\kappa_{11}}\right) e^{-j\kappa_{11}2d_1}\right) \cos\left(\beta_1^{TE} x\right) e^{-j\kappa_{11}z} \tag{4-7}$$

$$E_y(x, y=0, z)_{T-junction} =$$
$$u_{in} e^{j\frac{\pi}{4}} \frac{\sqrt{\lambda}}{4d_1 d_2} \left(D_{T1} + D_{T4}\Gamma e^{-j\kappa_{1,1}4d_1} - \left(D_{T2} + D_{T3}\Gamma e^{-j\kappa_{1,1}4d_1}\right)e^{-j\kappa_{1,1}2d_1}\right)\cos\left(\beta_1{}^{TE} x\right)e^{-j\kappa_{1,1}z} \tag{4-8}$$

$$E_y(x, y=0, z)_{L-junction} =$$
$$u_{in} e^{j\frac{\pi}{4}} \frac{\sqrt{\lambda}}{4d_1 d_2} \left(D_{L1} + (D_{L2} + D_{L3})\Gamma e^{-j4d_1\kappa_{1,1}}\right)\cos\left(\beta_1{}^{TE} x\right)e^{-j\kappa_{1,1}z} \tag{4-9}$$

where u_{in} is given by

$$u_{in} = E_y(x = \pm d_1, y = 0, z = L) = \left(\frac{-I_0 h}{4d_1 d_2}\right)\left\{\left(\frac{\omega\mu_0}{\kappa_{1,1}}\right)\cos\left(\beta_1{}^{TE}(\pm d_1)\right)e^{-j\kappa_{1,1}L}\right\} \tag{4-10}$$

and D_i is the UTD diffraction coefficient for (1,1) diffracted mode from (1,1) incident mode at corner for the width of $2d_1$ and the height of $2d_2$ tunnel.

The coupling loss for (1,1) mode can be defined by the ratio of the fields in main tunnel and side arm and results from corner diffraction. By (4-7) ~ (4-10) and (1,1) mode expression of (4-6), the coupling losses for three structures are showed in Figure 4-7.

$$CL_{cross} =$$
$$e^{j\frac{\pi}{4}} \frac{\sqrt{\lambda}}{4d_1}\left\{D_{C1} + D_{C2}e^{-j2d_1\kappa_1} - \left(D_{C3} + D_{C4}e^{-j2d_1\kappa_1}\right)e^{-j\kappa_1 2d_1}\right\}e^{-j\beta_1{}^{TE}d_1} \tag{4-11}$$

$$CL_{T-junction} =$$
$$e^{j\frac{\pi}{4}} \frac{\sqrt{\lambda}}{4d_1}\left\{D_{T1} + D_{T4}\Gamma e^{-j\kappa_1 4d_1} - \left(D_{T2} + D_{T3}\Gamma e^{-j\kappa_1 4d_1}\right)e^{-j\kappa_1 2d_1}\right\}e^{-j\beta_1{}^{TE}d_1} \tag{4-12}$$

$$CL_{L-junction} = e^{j\frac{\pi}{4}} \frac{\sqrt{\lambda}}{4d_1 d_2}\left\{D_{L1} + (D_{L2} + D_{L3})\Gamma e^{-j4d_1\kappa_1}\right\}e^{-j\beta_1{}^{TE}d_1} \tag{4-13}$$

where UTD coefficients for coupling losses are listed in Table 4-1.

	UTD Coefficient	Incident Angle	Diffracted Angle
Cross Tunnels (Figure 3-7)	D_{C1}	$\tan^{-1}\left(\frac{\lambda}{4d_1}\right)$	$\frac{3\pi}{2}-\tan^{-1}\left(\frac{\lambda}{4d_1}\right)$
	D_{C2}	$\frac{\pi}{2}+\tan^{-1}\left(\frac{\lambda}{4d_1}\right)$	$\tan^{-1}\left(\frac{\lambda}{4d_1}\right)$
	D_{C3}	$\tan^{-1}\left(\frac{\lambda}{4d_1}\right)$	$\frac{\pi}{2}+\tan^{-1}\left(\frac{\lambda}{4d_1}\right)$
	D_{C4}	$\frac{\pi}{2}+\tan^{-1}\left(\frac{\lambda}{4d_1}\right)$	$\pi-\tan^{-1}\left(\frac{\lambda}{4d_1}\right)$
T-junction Tunnels (Figure 3-11)	D_{T1}	$\tan^{-1}\left(\frac{\lambda}{4d_1}\right)$	$\frac{3\pi}{2}-\tan^{-1}\left(\frac{\lambda}{4d_1}\right)$
	D_{T2}	$\tan^{-1}\left(\frac{\lambda}{4d_1}\right)$	$\frac{\pi}{2}+\tan^{-1}\left(\frac{\lambda}{4d_1}\right)$
	D_{T3}	$\frac{\pi}{2}+\tan^{-1}\left(\frac{\lambda}{4d_1}\right)$	$\pi-\tan^{-1}\left(\frac{\lambda}{4d_1}\right)$
	D_{T4}	$\frac{\pi}{2}+\tan^{-1}\left(\frac{\lambda}{4d_1}\right)$	$\tan^{-1}\left(\frac{\lambda}{4d_1}\right)$
L-bend Tunnels (Figure 3-15)	D_{L1}	$\tan^{-1}\left(\frac{\lambda}{4d_1}\right)$	$\frac{3\pi}{2}-\tan^{-1}\left(\frac{\lambda}{4d_1}\right)$
	D_{L2}	$\frac{\pi}{2}+\tan^{-1}\left(\frac{\lambda}{4d_1}\right)$	$\tan^{-1}\left(\frac{\lambda}{4d_1}\right)$
	D_{L3}	$\tan^{-1}\left(\frac{\lambda}{4d_1}\right)$	$\frac{\pi}{2}+\tan^{-1}\left(\frac{\lambda}{4d_1}\right)$

Table 4-1 Incident and diffracted mode angles for UTD coefficient for coupling of (1,1) modes in the main and cross tunnels

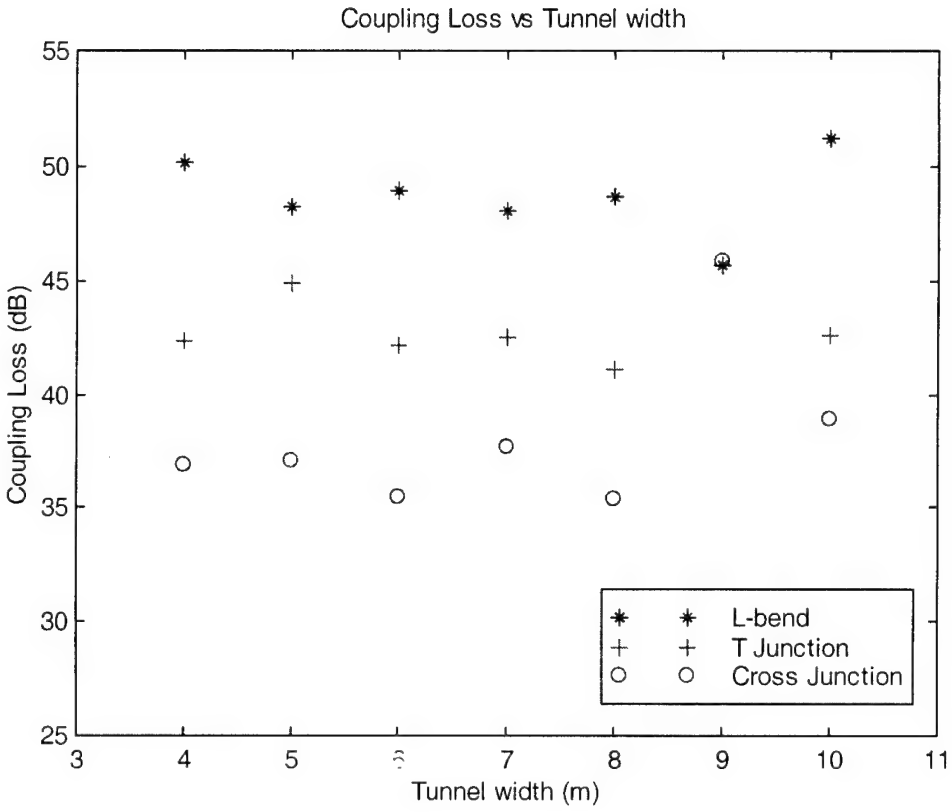

Figure 4-6 Coupling Loss vs Tunnel width by modal simulation

for Vertical Polarized 900MHz source
(Dielectric constant of walls =6)

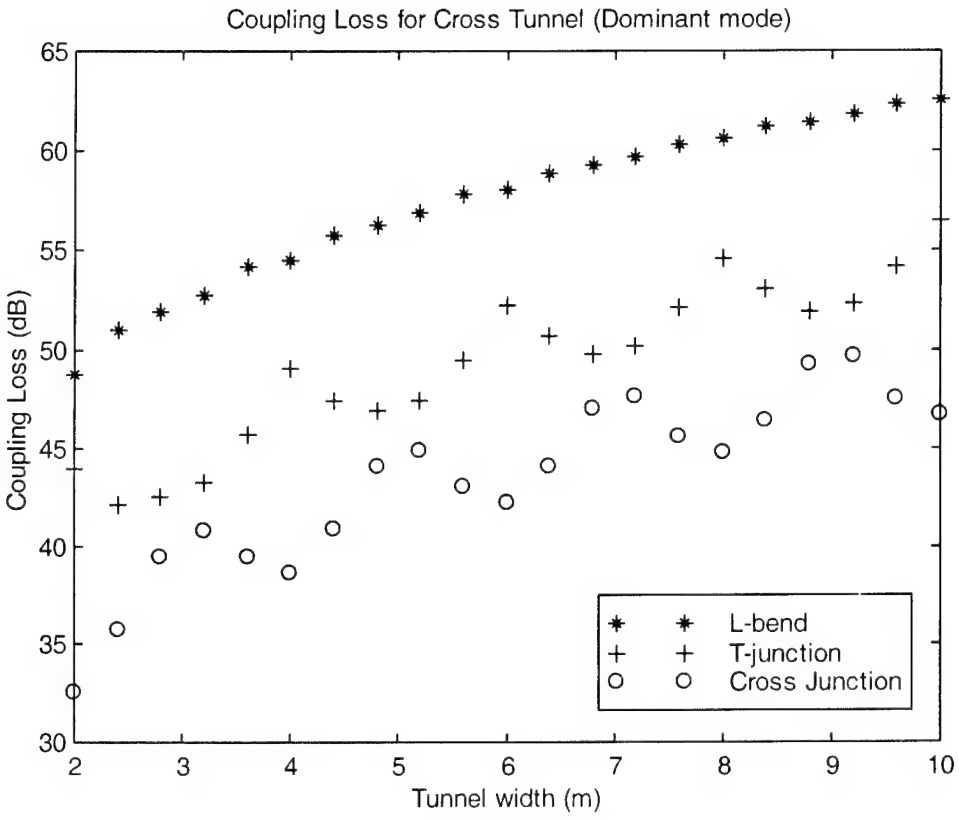

Figure 4-7 Coupling Loss vs Tunnel width for Dominant (1,1) modes for Vertical Polarized 900MHz source

(Dielectric constant of walls =6)

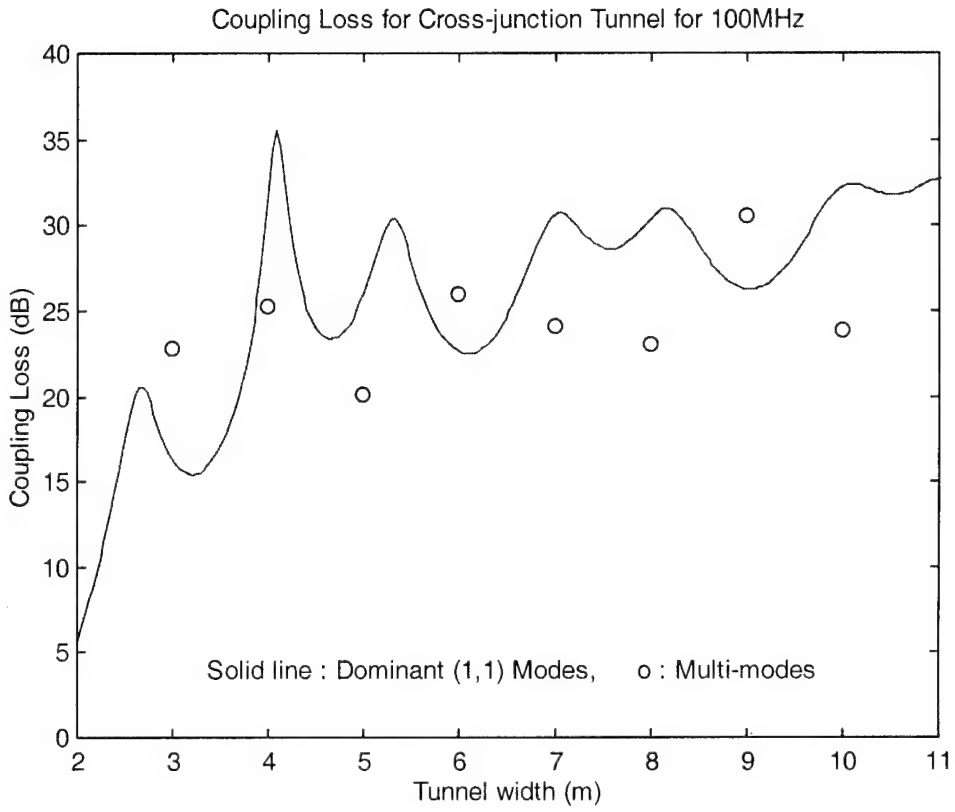

Figure 4-8 Coupling Loss vs Tunnel width for Dominant (1,1) modes and Multi-modes
Vertical Polarized 900MHz source (Dielectric constant of walls =6)

4.4 Comparison of coupling losses with measurements

The simulation results of each coupling loss of three junctions are compared with the measurements by Sakai et. al. [7]. They made three scaled tunnels by Bakelite slabs sandwiched between two metallic plates ($\varepsilon_r = 3.9$, $\varepsilon_i = 0.38$), the width of L-bend, T-junction and cross tunnels were 6 cm, 8 cm and 5 cm, respectively. Vertically polarized 9.45 GHz source was used, and they measured signal at middle of the other tunnel arm. To compare with these measurements, the width of the tunnels is fixed as 4 m, and the operating frequencies of each tunnel are 118 MHz for cross tunnel, 189 MHz for T-junction, and 141 MHz for L-bend tunnel with same dielectric constant of the walls for modal simulations. The coupling losses by measurements were 27 dB for cross tunnel, 32 dB for T-junction and more than 28 dB for L-bend tunnel. Using modal simulations, we have 20 dB for cross tunnel, 33 dB for T-junction and 30 dB for L-bend tunnel.

Other measurements by Emslie et. al. was for corner loss in high-coal mine cross tunnels (14 feet x 7 feet) [2]. The dielectric constant of the walls was said to be $\varepsilon_r = 10$. The measured coupling loss of 40 dB, and 42 dB for horizontally polarized fields at 415 MHz and 1 GHz. The modal simulation for these measurement obtained a coupling loss of 37 dB for 415 MHz and 40 dB for 1GHz. The results of these two sets of measurements indicate the validity of the modal expressions for prediction of coupling loss at tunnel junctions. The comparison is summarized in Table 4-2.

	Modal Analysis	Measurements
Cross Tunnel [7]	20 dB	27 dB
T-junction Tunnel [7]	33 dB	32 dB
L-bends Tunnel [7]	30 dB	more than 28dB
Cross Tunnel (415MHz) [2]	37 dB	40 dB
Cross Tunnel (1GHz) [2]	40 dB	42 dB

Table 4-2 Comparison of coupling loss with measurements [7],[2]

4. Conclusion

Radio propagation in long and narrow tunnels can be described using modal analysis. In over sized tunnels, there exists many modes but only a few lower modes are dominant for propagating to long distance from the transmitter because the higher attenuation constant of the higher modes. The attenuation constant in tunnels depends on the mode numbers, tunnel dimensions and frequency through the parameter $n^2\lambda^2/(2d_1)^3$ and $m^2\lambda^2/(2d_2)^3$, where n, m are mode numbers, λ is the wavelength and $2d_1$, $2d_2$ are tunnel width and height. The attenuation increases with wavelength (decreases with frequency) and mode number, and decreases with tunnel size. For tunnels that are wider than they are high ($2d_1 > 2d_2$), the modes with horizontal electric field have the least attenuation.

We have evaluated the modal coupling for tunnels with junctions using hybrid ray-mode conversion. The coupling mechanism is explained through mode diffraction at the corners into the side tunnels. We have found that the coupling loss is 50 dB for L bend junction, 42 dB for T junction and 37 dB for cross junction in 4m wide for 900 MHz signals that have vertical polarization. These coupling loss increases slightly with increasing tunnel width.

References

[1] Paul Delogne, "EM Propagation in Tunnels", IEEE tr. AP, vol. 39, no. 3, pp 401 – 406, Mar 1991

[2] A. G. Emslie, L. L. Robert, and P. F. Strong, "Theory of the propagation of UHF radio waves in coal mine tunnels", IEEE tr. AP, vol. AP-23, no. 2, pp. 192 – 205, Mar 1975

[3] D. Cichon, T. Zwick, and W. Wiesbeck, "Determination of Time-Variant Radio Links in High-Speed Train Tunnels by Ray Optical Modeling", IEEE AP-S , vol. 1, pp. 508 – 511, 1995

[4] D. Cichon, T. Zwick, and W. Wiesbeck, "Ray Optical Modeling of Wireless Communications in High-Speed Railway Tunnels", IEEE 46th VTC '96, vol. 1, pp. 546 – 550, 1996

[5] S. Chen and S. Jeng,"SBR Image Approach for Radio Wave Propagation in Tunnels with and without Traffic", IEEE tr. VT , vol. 45, no. 3, Aug 1996

[6] S.F. Mahmound and J. R. Wait, "Geometrical optical approach for electromagnetic propagation in rectangular mine tunnels", Radio Sci., vol. 9, no. 12, pp. 1147 – 1158, 1974

[7] K. Sakai and M. Koshiba, "Analysis of electromagnetic field distribution in tunnels by the boundary-element method", IEE Proc., vol. 137, Pt. H, no. 4, pp. 202 –208, Aug. 1990

[8] P. Mariage, M. Lienard and P. Degauque, "Theoretical and Experimental Approach of the Propagation of High Frequency Waves in Road Tunnels", IEEE tr. AP, vol. 42, no. 1, pp. 75 – 81, Jan. 1994

[9] H. Y. Yee, L. B. Felsen, and J. B. Keller, "Ray theory of reflection from the open end of a waveguide", SIAM J. App. Math., vol. 16, pp. 268 –300 , 1968

[10] Athanasios Papoulis ,Signal Analysis , McGraw-Hill, Inc. 1977

[11] Constantine Balanis, Advanced Engineering Electromagnetics, John Wiley & Sons 1989

[12] Raymond J. Luebbers, "Finite Conductivity Uniform GTD Versus Knife Edge Diffraction in Prediction of Propagation Path Loss", IEEE tr. AP, vol. 32, pp. 70 –76 , Jan. 1984

[13] Henry L. Beroni, Radio Propagation for Modern Wireless Systems , Prentice Hall PTR, 2000